Computational Study of Emergent Behavior in Active Matter Systems with Particle Shape

by

Shannon E. Moran

A dissertation submitted in partial fulfillment
of the requirements for the degree of
Doctor of Philosophy
(Chemical Engineering and Scientific Computing)
in The University of Michigan
2020

Doctoral Committee:

Professor Sharon C. Glotzer, Chair
Assistant Professor Jordan Horowitz
Associate Professor Xiaoming Mao
Professor Robert Ziff

Shannon E. Moran

moranse@umich.edu

ORCID iD: 0000-0002-3579-3149

To Mom and Dad.

ACKNOWLEDGEMENTS

Without you all, this PhD process would not have happened– thank you.

First, thanks goes to my advisor, Professor Sharon Glotzer. Thank you for setting an example of a creative, innovative, and impactful scientist that I've aspired to emulate.

One of the many things that has made my time at Michigan so special has been the support of the faculty and the collegial academic community. Professor Robert Ziff, I've so appreciated our chats about science, Ann Arbor, and life over the last few years. To my thesis committee– Sharon, Bob, and Professor Xiaoming Mao and Professor Jordan Horowitz– thank you for taking the time to improve this work before it went into print. Professor Lola Eniola, I'm so grateful for your mentorship these last few years as we worked together on the Peer Mentorship program. I learned a lot about working in academia, effecting change, and professional advancement from you.

Thanks is also due to mentors who helped get me to this point. Professor Matt Helgeson, thank you for taking on an enthusiastic undergrad and joyously showing me what it meant to do real science. Our venture to NIST for beam time in a blizzard was the moment I realized that I could be a scientist, and that moment of realization still brings me joy nearly 10 years later. Adam Rothman, thank you for supporting me in going back for a doctorate post-BCG. Five years after we last worked together, I still think back often on the lessons you taught me about management, passion for work, and my own leadership style.

My time in the Glotzer lab has been spent working on active matter. Thank you to the original "active matter subgroup" I had the pleasure of starting my PhD journey with– Isaac Bruss (a coauthor on the paper behind Chapter IV), Matthew Spellings, Chengyu Dai, and Mayank Agrawal.

My time in graduate school has been blessed by outstanding "co-workers" I could not have gotten through this time without. Will Zygmunt, thanks for keeping me laughing when I should have been working, for always being down for a walk and coffee, and for keeping me more grounded than I would have ever been without your friendship. As I've handed in my thesis before you: "Marco". Vyas Ramasubramani and Bradley Dice, how lucky I am to have worked with people whose company I so enjoy and who have been such technical role models for me. I'm a better computational scientist thanks to both of you. Karen Coulter, among many more impactful things I should list here, thank you for giving me the push I needed to take up hockey. MACHRL was one of the great joys of my time in grad school. Other colleagues-turned-friends, in alphabetical order– Rosy Cersonsky Adorf, Simon Adorf, Jim Antonaglia, Julia Dschemuchadse, Chrisy Du, Erin Teich– thank you keeping me laughing through this PhD process.

Thanks also goes to friends outside of the Glotzer lab who helped me keep an eye on the world outside of academia. Kavita Chandra, thank you for assuring me that I would eventually finish this thing (and for being a great friend, etc etc). Alison Banka, thanks for being my sounding board in grad school. I look forward to finding more chip dip recipes in common.

Finally, I would never have taken the step of coming to graduate school without the support of my family. Mom and Dad, thank you for always enabling me to push myself, for loving me, and showing me what it means to be a good person. Louie and Colin, being your sister has been one of the greatest gifts of my life. When I think of family, it's our trio that I think of. Last but not least– Alice, none of this would

have been possible without your unpaid labor as my editor-in-chief. What a gift it is to love and be loved by you.

This thesis is based upon work supported by the National Science Foundation Graduate Research Fellowship under Grant No. DGE 1256260. I also acknowledge financial support for my graduate studies as an ACM SIGHPC and Intel Computational and Data Science Fellow, and from the Point Foundation as a Point Scholar.

The projects in this work were supported as part of the Center for Bio-Inspired Energy Science, an Energy Frontier Research Center funded by the U.S. Department of Energy, Office of Science, Basic Energy Sciences under Award # DE-SC0000989. Work in Chapter IV was supported in part through computational resources and services supported by Advanced Research Computing at the University of Michigan, Ann Arbor. Work in Chapter IV and VI used resources of the Oak Ridge Leadership Computing Facility, which is a DOE Office of Science User Facility supported under Contract DE-AC05-00OR22725.Work in Chapters V and VI used the Extreme Science and Engineering Discovery Environment (XSEDE), which is supported by National Science Foundation grant number ACI-1548562; XSEDE award DMR 140129.[1]

TABLE OF CONTENTS

LIST OF FIGURES

Figure

ABSTRACT

Murmurations of birds, schools of fish, and herds of migrating animals are macroscale examples of self-propelled units exhibiting emergent collective behavior. We call such systems "active matter". On the colloidal scale, active matter systems of self-propelled particles exhibit a rich array of emergent phenomena with the potential for useful responsive and transport behaviors. A particularly intriguing aspect of active matter is that it is a non-equilibrium phase transition with no explicit equilibrium mapping, as active systems undergo phase separation from a sparse gas phase to a dense phase-separated regime even in the absence of explicit inter-particle attraction. One way of tailoring the interactions between particles without adding explicit interaction terms is to give particles shape, thereby adding steric effective interactions to the system. Understanding the role of effective interactions on the phase separation and emergent behavior in active matter systems will be of great utility as the field looks to engineer targeted behavior through particle and system design.

In this thesis, I computationally and theoretically describe the role of particle shape on the phase separation and emergent behavior of 2D self-propelled polygons in an active matter system.

In the first project, I perform a systematic study of the impact of particle shape on the phase separation behavior in active systems. I find that structure in the phase-separated cluster resembles that of the shape's densest packing in equilibrium systems. I develop a method for quantifying the impact of an effective interaction (e.g. shape) on the onset of phase separation in "collision efficiency", capturing the ability of inter-particle collisions to slow down particles during motility-induced phase separation (MIPS). Importantly, this also allows me to explain a previously-observed

steady-state "oscillatory" regime as a natural consequence of particle shape in active systems.

In the second project, I investigate a simple method of varying inter-particle collisions at a system level: through mixing particle types. I uncover emergent phenomena not yet seen in active Brownian particle systems, including microphase separation and stable fluid clusters that can coexist at steady state with solid clusters and a sparse gas phase. I quantify a measurable, implicit steric attraction between active particles as a result of shape and activity. This provides the first evidence that implicit interactions in active systems, even without explicit attraction, can lead to a calculable effective preferential attraction between particles. Importantly, that the narrow slice of system and particle design space I investigate still exhibits such rich emergent phenomena highlights the potential for a wide variety of behavior to be accessible to active matter systems through simple parameter designs.

In the third project, I take a fundamental approach to understanding the impact of particle shape in active systems by investigating whether systems of different self-propelled particles with shape fall into different universality classes. By mapping active matter near the order-disorder transition onto a non-equilibrium percolation model, I identify three distinct cluster evolution curve collapses of similar-behaving shapes. I further find that the quasi-critical behavior of the cluster scaling distribution predicts the same groupings as the collapsed cluster evolution curves. Further work will be needed to confirm the critical exponents, including a more rigorous finite size scaling approach to identify the critical point of each system.

CHAPTER I

Introduction

Active matter is a field of rapidly expanding interest and research activity over the last decade [4–7]. Vicsek's pioneering work showed a collection of point particles with alignment rules displays rich collective behavior, including phase separation [8]. However, theoretical work describing the collective behavior of bacteria demonstrates that phase separation behavior is not reliant upon explicit alignment rules [9]. In a phenomenon known as "motility-induced phase separation" (MIPS), systems of disks were found to phase separate as a consequence of density-dependent particle velocity [10]. This phase separation behavior of isotropic particles has been explained using a variety of models, including: athermal phase separation [11], the kinetic steady-state balancing of particle fluxes [12, 13], classical nucleation [14, 15], and the balancing of collision and ballistic timescales [16]. Importantly, phase separation predicted by theory has been observed in experiments, which confirm the activity-dependent formation of clusters and "active crystals" [17–19].

In real-world systems, particles (e.g. bacteria) are rarely isotropic in shape. Thus, one thrust in the active matter community has focused on understanding how particle anisotropy will change the behavior theoretically predicted for systems of isotropic particles. In a simple anisotropic model, simulations of rods with varying aspect ratios and densities display a rich variety of collective motion, such as laning, swarming, and

jamming [20–22]. Additionally, simply changing the direction of the driving force relative to a fixed particle shape drastically alters the resulting collective behavior and onset of phase separation [23, 24].

Few general mechanisms have been proposed for the impacts of particle anisotropy, which can lead to a variety of emergent behaviors. Active squares display a steady state "oscillatory" regime in which large clusters break up and re-form [25]. Mixtures of gear-shaped "spinners" with opposite rotational driving forces phase separate through competing steric interactions [26–28]. In systems of active "dumbbells", particle anisotropy allows for the stabilization of cluster rotation [29, 30]. This cluster rotation is also observed in active squares [25], but is notably absent in clusters of frictionless isotropic particles.

From these studies, we can see a general description of the impact of particle shape anisotropy on the phase separation and emergent system behavior is needed. Such a description would allow us to tailor the form and onset of critical behavior in active systems through "implicit" steric means, rather than explicit interaction rules.

In this thesis, I computationally and theoretically describe the role of particle shape on the phase separation and emergent behavior of 2D self-propelled polygons in an active matter system. This thesis is organized as follows.

In Chapter II, I provide an overview of the progress in designing systems of active, self-propelled particles and theoretical descriptions of their critical and emergent behavior motivating this work. In Chapter III, I outline the 2D active polygon model and dynamics I use for Chapters IV-VI.

In Chapter IV, I perform a systematic study of the impact of particle shape on the phase separation behavior in active systems. I find that structure in the phase-separated cluster resembles that of the shape's densest packing in equilibrium systems. I develop a method for quantifying the impact of an effective interaction (e.g. shape) on the onset of phase separation I call "collision efficiency", capturing

the ability of inter-particle collisions to slow down particles during motility-induced phase separation (MIPS). Importantly, this also allows me to explain a previously-observed steady-state "oscillatory" regime as a natural consequence of particle shape in active systems.

In Chapter V, I investigate a simple method of varying inter-particle collisions at a system level: through mixing particle types. I uncover emergent phenomena not yet seen in active Brownian particle systems, including microphase separation and stable fluid clusters that can coexist at steady state with solid clusters and a sparse gas phase. I quantify a measurable, implicit steric attraction between active particles as a result of shape and activity. This provides the first evidence that implicit interactions in active systems, even without explicit attraction, can lead to a calculable effective preferential attraction between particles. Importantly, that the narrow slice of system and particle design space I investigate still exhibits such rich emergent phenomena highlights the potential for a wide variety of behavior to be accessible to active matter systems through simple parameter designs.

In Chapter VI, I take a fundamental approach to understanding the impact of particle shape in active systems by investigating whether systems of different self-propelled shapes fall into different universality classes. By mapping active matter near the order-disorder onto a non-equilibrium percolation model, I identify distinct cluster evolution curve collapses of similar-behaving shapes. I further find that the quasi-critical behavior of the cluster scaling distribution predicts the same groupings as the collapsed cluster evolution curves. Further work will be needed to confirm the critical exponents, including a more rigorous finite size scaling approach to identify the critical point of each system.

The work in this thesis opens a variety of intriguing questions about the potential for effective interactions to be a rich avenue for engineering active matter systems. I conclude with thoughts on future work in Chapter VII.

This thesis contains work that is currently in preparation or undergoing peer review. The results contained in Chapter IV have been submitted for peer review, while the projects reported in Chapters V and VI are currently in preparation.

CHAPTER II

Background

The work in this thesis samples from and builds upon a wide foundation of theoretical work in active matter. After motivating this study by highlighting potential applications of active matter as currently theorized, I propose a framework for understanding the potential of active matter engineering and where this thesis adds to that body of work.

2.1 Why active matter, matters

Active matter's non-equilibrium nature means it is not bound by the typical restrictions on equilibrium material systems. Harnessing the potential for directed, responsive motion, we could look to engineer colloidal-scale systems with the ability to transport materials, respond to stimuli, or do work on a system [31, 32]. Thoroughly understanding the impact of design choices on system behavior while developing theoretical bases for future design is an overarching goal for the field, and motivates the framework for design choices presented below.

2.2 Framework for design of active matter systems

As we look to design active matter systems, a framework for the degrees of design freedom is needed. I propose such a framework in Figure 2.1, and expand upon the

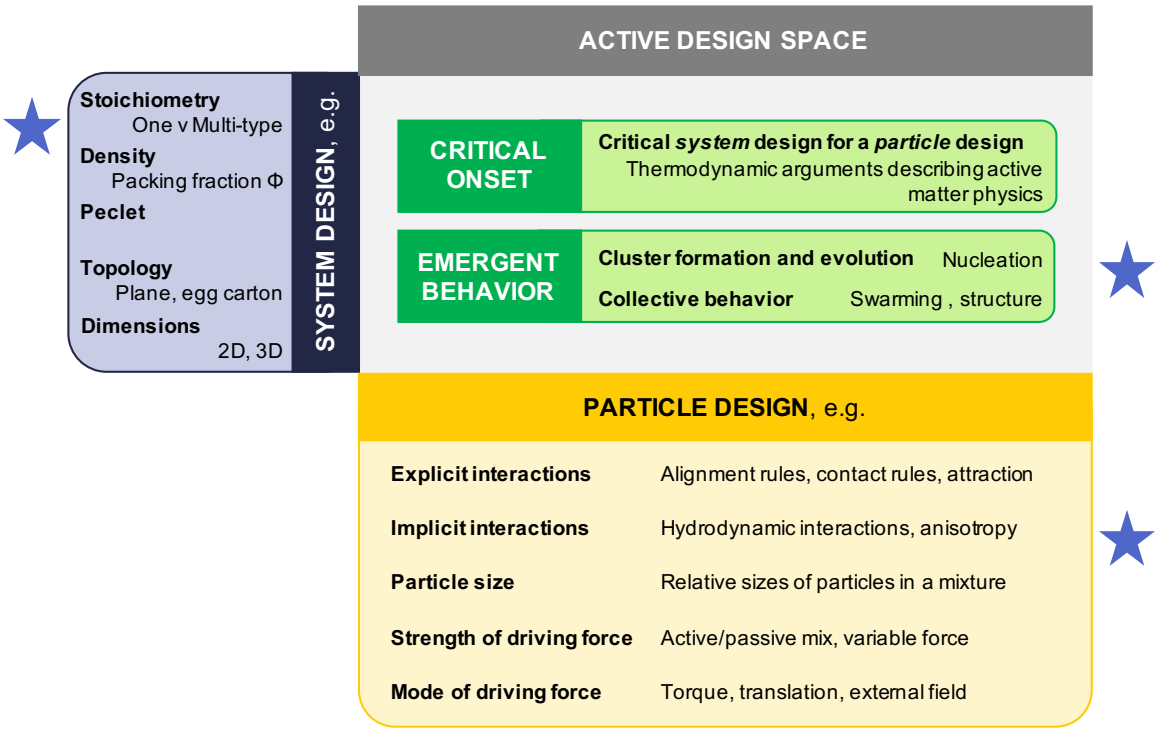

Figure 2.1: The design space for active matter can be broken into two components: System Design and Particle Design. In changing aspects of these two design components, we seek to engineer the Critical and Emergent Behavior a system exhibits. In this thesis, I vary (indicated by the blue stars) the stoichiometry (in the creation of a 2-component mixture) and implicit interactions (shape) and identify emergent behaviors not previously seen in active matter systems. The discovery of novel active behavior by tuning just a narrow set of parameters in this space highlights the richness of this design space, and the opportunity for further theoretical work to understand the role of System and Particle Design on system behavior. (Seminal citations for each design component and target behavior are included in the text.)

key aspects of design and targeted behavior in the sections following. This review of the literature is meant to be representative by highlighting foundational work in the field.

2.2.1 System design of active systems

Stoichiometry: By "stoichiometry", we also include the inclusion of two components in a system. Such mixtures have included mixtures of particles with varying speed [33], different force directors [23], or rotational directions [28]. Studies have also used small numbers of active particles to effect structural change on a medium [34–36].

Density and Péclet: Phase separation diagrams and theories have largely been developed as a function of these two parameters [11–16, 37].

Topology: Much of the theoretical work describing phase separation in isotropic active particles has focused on motion on flat surfaces. However, curvature can also impact the behavior of active systems. Microswarming on a sphere is curvature dependent, with areas of preferential clustering on surfaces of non-constant curvature [38]; an ellipsoid surface was used to change the emergent behavior of a nematic system [39]; vorteces and polar bands are found on a sphere [40]; and curvature-induced vortices occur on an ellipsoid [41]. Activity and curvature remains an area ripe for further exploration.

Dimensions: Though much theory was first developed in 2D, research has shown that the onset of phase separation in 2D and 3D occurs at different system densities [10, 16].

2.2.2 Particle design of active systems

Explicit Interactions: The pioneering example of active matter is Tamás Vicsek's pioneering work on a system of point particles with explicit neighbor alignment

rules [8]. In addition to such specific alignment rules, we can also envision systems which have explicit rules upon particle interaction such as slowing upon contact [42] or proximity-induced attractions [43]. Such attraction can also be variable, such as chemotaxis and other sensing behaviors such as those seen in bacteria [44]. Interactions also need not be reciprocal between particle types.

Implicit Interactions: As has been suggested by the title of this thesis, shape is a particularly interesting type of implicit interaction. By "implicit", we mean here that there is not a clearly defined set of interaction rules. Instead, behaviors arise as a result of individual particle properties. As examples: systems of rods of varying aspect ratios display laning, swarming, and jamming [20–22]; active squares display a steady state "oscillatory" regime in which large clusters break up and reform [25]; mixtures of gear-shaped "spinners" with opposite rotational driving forces phase separate through competing steric interactions [26–28]; and systems of active "dumbbells" stabilize cluster rotation [29, 30].

Other types of implicit interactions may be non-specific results of particle motion. One example is particle hydrodynamics, which may be thought of as a non-specific implicit interaction and is well-studied in active matter [5].

Particle size: Relative particle size can impact the other aspects of a particle design's ability to interact. Active depletants can be implemented as active disks which can induce effective interactions on large passive particles [45]. Systems of particles of polydisperse size can exhibit a glassy, rather than solid, phase-separated regime [46].

Strength of driving force: While passive/active mixtures are mentioned elsewhere in this framework, the ability to modulate the strength of a particle's driving force is its own powerful design lever. To recall a few specific examples, active particles can help shepherd passive particles [33], pin dislocations in crystals [34], and anneal grain boundaries in a passive colloidal crystal [36].

Mode of driving force: In this thesis I will focus solely on self-propelled translational active matter. However, entire fields of active matter explore particles in external fields, periodic external fields, rotational active matter, and run and tumble particles, to name a few [4, 5]. While some of the fundamental interactions may be similar across these classes of behavior, it is not immediately obvious that the same theoretical foundations will apply.

2.3 Theoretical understanding of active matter

Design of active particles would allow us to tailor two specific types of behavior: the onset of phase separation (distinct from a critical point, but what we will call critical onset) and emergent collective behavior. While experimentation can shed light on the behavior of specific systems, theoretical frameworks allow us to understand and potentially predict the behavior of systems in lieu of experimentation.

We highlight key theoretical work below. We note that a key limitation in these theories is that they do not offer ways of accounting for experimental conditions, e.g. hydrodynamic interactions of swimming particles [17]. We would expect to need to add correction factors to theories to be able to theoretically calculate precise behavior predictions (e.g. critical density).

2.3.1 Critical onset

The dominant explanation for phase separation in active Brownian particles is that of "motility-induced phase separation" (MIPS) [10]. In this foundation work, a density-dependent particle velocity leads to an emergent slowing of particles in areas that become clusters. I will directly build on this theory in Chapter IV.

Additional theories have taken a variety of approaches to describing the phase behavior, including: describing the phase separation as the consequence of an athermal clustering instability [11], kinetic steady-state balancing of particle fluxes [12, 13],

and classical nucleation [14, 15].

Two other theories are worth highlighting here as bases for work in this thesis. A collision theory based argument balances the time scales of ballistic movement and collision time to back out the phase separation behavior [16]. We will borrow this mapping of active matter onto collision theory for rescaling the timescales of our simulations in Chapter VI. Additionally, a propulsion-induced swim pressure has been used to develop thermodynamic arguments for active matter, including descriptors of phase separation onset [37]. The concept of a pressure induced through particle collisions is one we will adapt in our calculation of "collision efficiency" in Chapter IV.

2.3.2 Emergent behavior

We have already highlighted some interesting emergent behavior due to shape interactions above while discussing implicit interaction particle design. However, systems of particles with explicit interactions can also exhibit a wealth of emergent behavior: contact triggered active particles exhibit traveling waves, 4- or 6-fold order, and coexisting domains [43]; a system in which particles stop upon colliding with another particle can form fractal-like structures [42]; and even the original Vicsek model exhibited spontaneously selected system directionality [8].

CHAPTER III

Computational methods

A common particle model was used for all studies in this thesis, and is described here. Any changes to this particle model are noted in the respective chapters. The analytical methods, which are the major contributions to this thesis, are also summarized in their respective chapters.

3.1 Particle model

The model particles used in this thesis are shown in Figure 3.1. We study a family of regular polygons of side number $3 \leq n \leq 8$. Particles interact through a frictionless, purely repulsive, excluded volume Weeks-Chandler-Anderson (WCA) potential, $U(r) = 4\epsilon[(\sigma_{\mathrm{WCA}}/r)^{12} - (\sigma_{\mathrm{WCA}}/r)^{6}] + \epsilon$ for $r < r_{\mathrm{cut}}$, where $\sigma = 2r_{\mathrm{WCA}}$, $r_{\mathrm{cut}} = 2^{(1/6)}\sigma_{\mathrm{WCA}}$, and the radius of the potential $r_{\mathrm{WCA}} = 1$ for all simulations [47]. This r_{WCA} introduces an effective "rounding" to each shape about the vertex points. We set particle side length a to maintain a constant "side-to-rounded-corner" perimeter ratio, ζ, to $\zeta = \frac{\sum_s a_s}{2\pi r_{\mathrm{WCA}}} = 9$ over all sides s. We know from equilibrium studies [48–50] and other works on active anisotropic particle systems [25] that self assembly and critical behavior is sensitive to the effective "roundness" of particle vertices. As the repulsive interaction introduces a slight "rounding" to the shapes, maintaining a constant ζ over all simulations ensures our systems can be compared with one an-

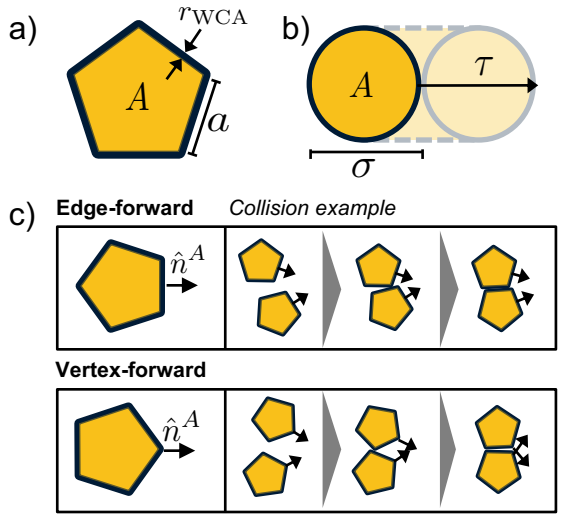

Figure 3.1: (a) Shape anisotropy is studied with a family of regular polygons of side length a. Here we show a pentagon as example. Particles interact through a purely repulsive WCA potential characterized by r_{WCA}. (b) Simulation timescales are characterized by τ, the time for a particle to ballistically travel its characteristic length, σ, calculated as the diameter of an equiarea (A) disk. (c) Force anisotropy is defined by the active force director, $\hat{n}^A$, which propels the shape either edge- or vertex-forward. A key feature of this system is that collisions of anisotropic particles can sustain translational and/or rotational motion. Illustrative collisions are provided for each force director.

other. This value $\zeta = 9$ was chosen to balance shape fidelity (less rounding) and simulation feasibility with computational demands.

We also explore anisotropy in the constant active force director ($\boldsymbol{F}_i^A = v_0 \hat{n}_i{}^A(\cos\theta_i, \sin\theta_i)$) applied to each particle i. For a given simulation, we set $\hat{n}_i$ to be either perpendicular to a side of the particle (*edge-forward*) or bisecting a vertex (*vertex-forward*), as shown in Figure 3.1c. The active force director $\hat{n}_i$ is initialized randomly for each particle from the set of possible vertex-forward or edge-forward directions for each simulation, and is locked in the particle's frame of reference. The active force direction changes only with particle rotation due to thermal fluctuations and collisions.

We took further care to ensure consistent anisotropy through our choice of active

force magnitude and temperature. Our systems were run at Péclet (Pe) number of Pe = 150, where Pe is a measure of active (advective) to diffusive motion (Pe = $\frac{v_0\sigma}{k_BT}$, where σ is the diameter of an equi-area disk for a given shape). In this Pe regime, we can treat the active driving force as the primary contributor to particle motion over thermal fluctuations. By setting the temperature of the thermal bath governing the fluctuations to $k_BT = \frac{v_0\sigma}{\mathrm{Pe}}$ and the magnitude of the active driving force $v_0 = 1$, we ensure that the interaction distance between interacting particles remains constant for all simulations.

Particle motion was solved for using the Langevin equations of motion.

$$m_i\dot{\boldsymbol{v}}_{\boldsymbol{i}} = \sum_j \boldsymbol{F}_{ij}^{Ex} - \gamma \cdot \boldsymbol{v}_{\boldsymbol{i}} + \boldsymbol{F}_i^A + \boldsymbol{F}_i^R \tag{3.1}$$

$$m_i\ddot{\theta}_i = \sum_j \boldsymbol{T}_{ij}^{Ex} - \gamma_R \cdot \boldsymbol{\omega}_{\boldsymbol{i}} + \sqrt{2\mathcal{D}_{\mathcal{R}}}\eta(t)_i^R \tag{3.2}$$

Mass (m_i) is set to 1×10^{-2} such that the dynamics closely approximate the Brownian limit in line with the expected dynamics of bacteria and colloidal-scale particles. The forces and torques due to excluded volume ($\boldsymbol{F}_{ij}^{Ex}$ and $\boldsymbol{T}_{ij}^{Ex}$) were calculated using a discrete element method [51], which calculates interparticle interactions between a point on one particle perimeter and a point on another particle's perimeter. Translational and rotational velocities are given by v_i and ω_i, respectively. We parametrized the implicit solvent via the translational drag coefficient $\gamma = 1$ and $\gamma_R = \frac{\sigma^3\gamma}{3}$ per the Stokes-Einstein relationship. These parameter choices correspond to the overdamped, diffusive limit. Our model does not account for solvent-mediated hydrodynamic interactions between active particles. Although there is a small inertial component in our model, we confirmed that it is not critical for any of the observed behavior. The last term in both equations accounts for thermal fluctuations. Noise is included via Gaussian random forces $\boldsymbol{F}_i^R = \sqrt{2\gamma k_BT}\eta(t)$ that model a heat bath at temperature T. Here $\eta(t)$ are normalized zero-mean white-noise Gaussian processes ($\langle\eta_i(t)\rangle = 0$ and

$\langle \eta_i(t)\eta_j(t')\rangle = \delta_{ij}\delta(t-t')$). This ensures thermodynamic equilibrium in the absence of the externally applied forces ($\boldsymbol{F}_{ij}^{A}$).

3.2 Dynamics and simulation methods

The area fraction covered by N particles was calculated as $\phi = \frac{NA_i}{A_{\text{box}}}$, where the area A_i of particle i includes both the hard shape and the rounding of $r_{\text{WCA}} = 1$ induced by the WCA potential. Each simulation contains $N = 1 \times 10^4$ particles in a square simulation box with periodic boundaries, with box size chosen to achieve the desired density.

The timescale of the simulation, τ, is the time for a particle to ballistically travel its own diameter ($\tau = \frac{\sigma\gamma}{v_0}$). The Langevin equations of motion were numerically integrated using a stepsize of 1×10^{-3}, chosen to balance efficiency with simulation stability. Particle positions were randomly initialized and allowed to relax with a repulsive isotropic potential between particle centroids at $\phi = 0.10$ for 5×10^5 time steps. This isotropic potential was then turned off and the WCA excluded volume potential between particle perimeter points was turned on while the box was slowly compressed to the target system density over 5×10^5 time steps. Only after these initialization steps was the active force turned on and the simulation run for 5000τ.

We assert that the simulations have reached steady state when the total system inter-particle collision pressure has reached a constant value. Ten replicates were run at each statepoint to provide sufficient statistics.

Simulations were run using the open-source molecular dynamics software HOOMD-blue (v2.2.1 with CUDA 7.5). The Langevin integrator uses a velocity-Verlet implementation [52]. Simulations were performed on graphics processing units (GPUs) [52, 53]. Shape interactions were modeled using the discrete element method implementation in HOOMD-blue[51] using an optimized rigid body routine for particle rotations[53]. The isotropic repulsive potential during initialization was implemented

using the dissipative particle dynamics (DPD) pair force implemented in HOOMD-blue[54].

3.3 Open source software used

The open-source simulation software HOOMD-blue, mentioned above, was used to perform the Molecular Dynamics simulations that form the basis of this work [52, 53].

Additional open source software managed within the Glotzer group was critical to completion of this work. Clustering, density, and nearest neighbor analyses (as detailed in later chapters) were implemented with Freud [55]. Data and simulation workflows were managed using the `signac` framework [56]. File format management was performed using the `garnett` package[1].

The open source Python community also provided packages instrumental to performing the analysis here, including Jupyter notebooks[57] and the `scipy`[58] and `numpy`[59] packages.

Simulation data in Chapter IV were visualized using Plato[2] and Chapter IV-VI were visualized using Ovito[2].

[1] https://garnett.readthedocs.io/en/stable/
[2] https://github.com/glotzerlab/plato

CHAPTER IV

Self-propelled Particle Shape Tailors Phase Separation Onset Through Effective Interactions

This chapter is adopted with minor modifications from a manuscript with co-authors Isaac R. Bruss and Sharon C. Glotzer.

Note that in this chapter, the "critical density of phase separation" refers to the density at which phase separation occurs under the given parameters of $Pe = 150$ (with calculations detailed in Section 4.2.1). This is not to be confused with the true critical density in Pe/Φ space.

4.1 Introduction

In this chapter we aim to develop a generalized description of the role of active particle anisotropy through direct comparison to frictionless active disks (i.e. isotropic particles). We study a family of translationally self-propelled 2D polygons (of side number $3 \leq n \leq 8$) with force director anisotropy implemented as shown in Figure 3.1. This choice of shapes systematically extends previous studies on triangles with inertia [23], triangles with friction [24], and squares [25]. Full simulation parameters and additional details can be found in Section 4.2 and Chapter III.

We show that the onset of phase separation at a critical density ϕ^* is highly

dependent on the shape of the particle given constant Pe. In our system, we observe phase separation at densities as low as $\phi^* = 0.01$ in vertex-forward 6-gons, or as high as $\phi^* = 0.37$ in edge-forward 3-gons– both below and above ϕ^* of disks. Interestingly, we find that the direction of the force director is sufficient for changing the ϕ^* for a given shape, but not for changing the relative phase separation onset between different shapes. Specifically, edge-forward active particles have higher ϕ^* than their vertex-forward counterparts. Additionally, the internal structure of the phase-separated cluster is primarily determined by the particle shape and resembles each shape's equilibrium densest packing. This resemblence suggests a link between structure and critical density not yet explored in active systems.

In addition to this systematic study, this work's contribution to the study of anisotropic active matter is the introduction of a "collision efficiency" measure. We find that systems with the lowest critical densities are also those that maximize particle deceleration per unit increase in inter-particle collision pressure, P_{coll}. That is, some shapes can more efficiently convert particle collisions into decreases in particle velocity, v, leading to phase separation. This allows us to quantitatively attribute changes to ϕ^* in systems of shapes versus disks to steric impacts on collisions, and directly shows that we can tune critical behavior of active systems by tuning the nature of the inter-particle collision dynamics.

We note that 3- and 4-gons (the only two previously studied active polygons) behave fundamentally differently from other polygons. We attribute this to the slip planes present in their densest packings. As these shapes have been used as model systems for a number of previous studies [23–25], we show why such results should not be generalized to systems that do not have slip planes.

4.2 Analysis Methods

4.2.1 Phase separation density calculation

Multiple methods exist in the literature to determine the critical density for phase separation in active systems. In an active system of squares[25], a system was considered "clustered" if the fraction of system particles in the largest cluster was $\geq$0.2. However, we found this method to be ill-suited for our systems, some of which are comprised of many small clusters. In disks, studies have used local-density histograms about randomly-sampled points of the simulation box [16] or about each particle [13]. If the histogram displayed two peaks, the system was considered phase separated. However, the very low system densities studied here limit the efficacy of the random-sample approach (e.g. at a packing fraction of 0.01, the high-density "peak" would be $\leq$2% of the magnitude of the larger peak). In dumbbells, studies used both a grid-based and Voronoi-based local density calculation to develop local density histograms, to equal effect [60].

To determine phase separation even at low densities, we calculated two separate histograms of local densities within a $2.5r_{\max}$ radius (1) of randomly sampled points ($N = 1 \times 10^5$) and (2) about each particle ($N = 1 \times 10^4$). For each shape, $r_{\max}$ was calculated as the circumscribing radius about the shape. We then calculated a position-normalized local density histogram of the system by multiplying the frequencies of local densities in each local density bin by one another. If the resulting histogram has a high-density peak $\geq$20% the height of the low-density peak, we consider the system to be phase separated.

The onset of this phase separation is characterized by a critical particle density, ϕ^*, at which the system transitioned from a homogeneous mixture to coexisting low and high density phases. We define the critical density, ϕ^*, as the lowest density at which $>$ 50% of the system replicates phase separate. In Figure 4.1, error bars are given

as the range of densities which have some replicates exhibiting both homogenous and with others exhibiting phase-separating behavior.

4.2.2 Structural order in clusters

We examine internal cluster structure with two order parameters. We first calculated the k-atic order parameter, i.e. the bond-orientation order parameter for k-fold rotational symmetry.

$$\psi_k(i) = \frac{1}{n}\sum_{j}^{n} e^{ki\theta_{ij}} \tag{4.1}$$

The parameter k governs the symmetry of the order parameter while the parameter n governs the number of neighbors of particle i to average over. For calculating bond order, θ_{ij} is the angle between the vector r_{ij} and $(1, 0)$, i.e. the angle of the bond between particle i and particle j with respect to the x-axis. In other systems, ψ_k has been used to identify hexagonal ($k = 6$) order in systems of active disks [13] and ordering on a square lattice ($k = 4$) in systems of active squares [25].

The body-orientation order parameter tells us relative *orientations* of local particles,

$$\xi_s(j) = e^{is\theta_j} \tag{4.2}$$

taking into account s-fold symmetry, where θ_j is the angle that rotates particle j from a reference frame into a global coordinate system and i is the imaginary unit. For particles with even n, $s = n$; for particles with odd n, we set $s = 2n$ to account for anti-parallel packings [61].

4.2.3 Collision pressure calculation

In a 2D system of particles, we used HOOMD (v2.2.1) to calculate the instantaneous (scalar) pressure of the system as $P = (2K + 0.5W)/A$, where K is the total kinetic energy, W is the configurational component of the pressure virial, and

A is the area of the box. We can isolate the pressure due to inter-particle collisions, $W/A = \frac{1}{2A}\sum_i \sum_{j \neq i} \boldsymbol{F_{ij}} \cdot \boldsymbol{r_{ij}} = P - \frac{2K}{A}$. We further normalize the pressure by the thermal energy as $P_{\text{coll}} \equiv (W/A)/k_BT$ to facilitate comparison among systems of particles, as k_BT is varied by shape to maintain constant Pe = 150. While pressure in equilibrium systems is typically taken over an ensemble, here we use it as an instantaneous measure of the location in configuration space of the system. This allows us to view particle trajectories in velocity and configuration space, allowing for the definition of a unique master curve for each system.

To calculate each shape's "trajectory" through v/P_{coll} space shown in Figure 4.10, we sampled complete simulation trajectories for simulations below, at, and above the critical density, and calculated a distinct P_{coll} and average particle velocity $\langle v \rangle$ for each time step. We then binned the P_{coll} values into equal-size bins, and calculate an overall average $\langle v \rangle$ and standard deviation of $\langle v \rangle$ for each bin. These averages and standard deviations are normalized by the $v_{\text{ballistic}}$ calculated for each shape, and are plotted against the average P_{coll} value in the corresponding bin.

4.3 Impact of particle shape on the system density of phase separation onset

As we increase the number of vertices (i.e. become more "disk-like"), we expected to see monotonically increasing critical density[62] from lower critical densities of high-anisotropy 3-gons towards higher critical densities of lower anisotropy 8-gons.

Instead, as shown in Figure 4.1a, phase-separation behavior does not vary monotonically with n. For shapes of $n = [3, 4]$, we observe a ϕ^* near that of disks in this Pe regime, with exact value dependent on the force director. As we increase n to 5, we see a sharp decrease in ϕ^* with continued dependence on the force director. The lowest critical densities are observed for shapes of $n = 6$, above which we observe the

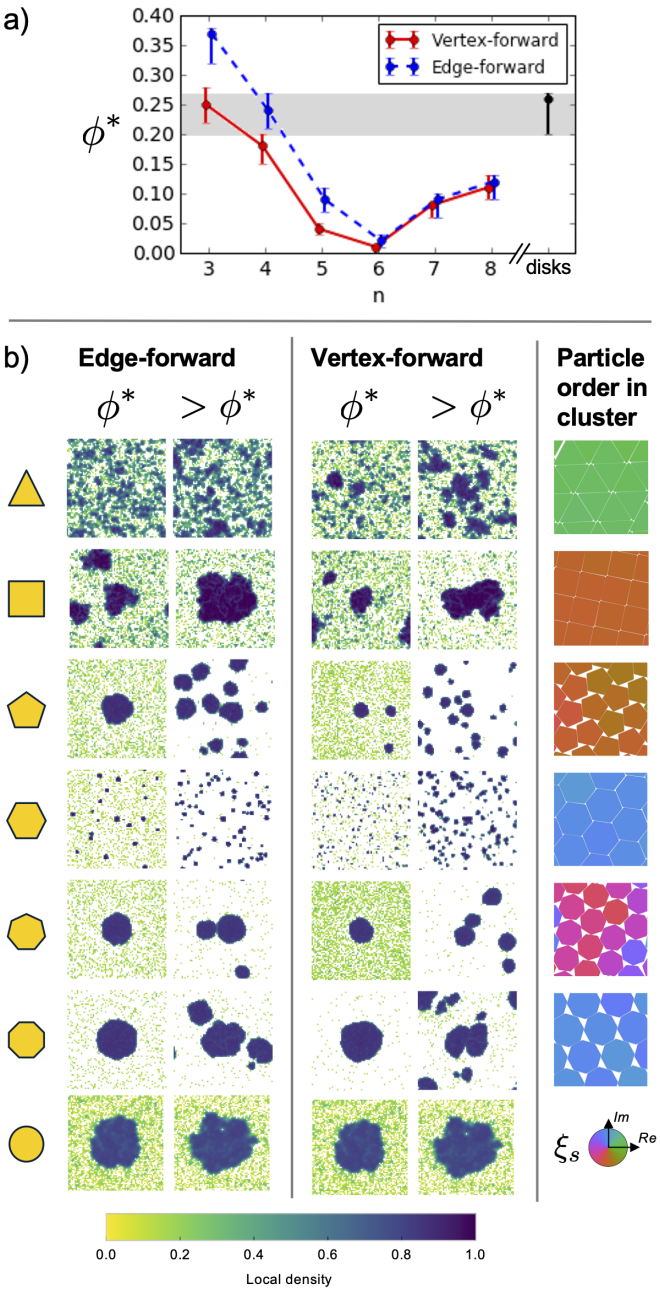

Figure 4.1: Critical density and collective behavior of active anisotropic systems. (a) Critical density for systems of each n-gon, calculated as described in Section 4.2.1. Lower error bar bounds indicate the minimum system ϕ at which at least one replicate phase separated, while the upper error bar bounds indicate the minimum ϕ at which all replicates phase separated. (b) Representative steady-state local density snapshots in the critical (ϕ^*) and phase separated ($> \phi^*$) regimes. A distinctive feature of phase separation in systems of anisotropic particles is the formation of multiple stable clusters that persist for long time scales. A representative snapshot of particle orientation in the cluster is shown in the far right column.

expected monotonic increase in ϕ^* as n is increased to [7,8].[63]

We first address the impact of the force director. We expect ϕ^* to depend on the nature of the active force director because the stability of small cluster depends on the force directors, as suggested in the collision example diagram in Figure 3.1. Specifically, for vertex-forward shapes, the only stable dimer sustains translational motion. For edge-forward shapes, stable dimers exist that are either stationary and/or can sustain translational motion. Looking only at the mechanical force balance on configurations of edge- versus vertex-forward particle clusters, we might expect that edge-forward particles would phase separate more easily due to more effective inter-particle slowing. However, the sustained translational motion of small clusters allows increased inter-cluster collisions in the vertex-forward systems. It is clear that this increased inter-cluster collision phenomena wins out, with lower ϕ^* for vertex forward $n = [3, 4, 5]$. Following this logic, the translational speed of a vertex-forward dimer relative to the particle ballistic velocity should decrease with increasing n. We hypothesize that for $n > 6$, this decrease in small cluster translational speed leads to the lack of difference between edge- and vertex-forward ϕ^*. Representative small-N clusters are shown for each combination of n-gon and force director in Figure 4.2.

In investigating the structures formed by particles in the phase-separated cluster, we find that without exception the particles have assembled into their densest packing, as shown in the far right column of Figure 4.1b. Using this information, we make the following observations. For 6-gons (the shape with the lowest ϕ^*), the densest packing has neither void space nor slip planes. For 5-, 7-, and 8-gons, the densest packing has void space, but no slip planes. For 3- and 4-gons, the densest packing has no void space, but has slip planes. In the context of this system of 2D polygons, a slip plane refers to a plane along which two otherwise undisturbed grains can slide in opposing directions. This leads us to hypothesize that a system's ability to inhibit particle movement in the cluster (where void space and slip planes play a role) is

critical to understanding the critical behavior.

Additionally, the only two shapes in our simulations that exhibit an "oscillatory" regime in their phase behavior are 3- and 4-gons (See Video Figures 4.4,4.5). These shapes are also the only two that have slip planes in their densest packings. In the literature, other studies have noted oscillation as novel behavior accessed via anisotropy and activity [25, 64]. We posit that the oscillatory regime for anisotropic particles is in fact a natural consequence of the preferred steady-state structure of the component particle shapes in these systems. We will revisit this claim more rigorously in Section 4.5.

Our final observation on the critical behavior is that the nature of the phase separation varies significantly based on shape, as shown in Figure 4.1b. Beyond the critical regime, we see the formation of many stable clusters at steady state for $n \geq 5$ (See Video Figures 4.6,4.7). This is in contrast to systems of isotropic disks, where secondary cluster formation is short-lived with phase separation characterized by a single large cluster [12, 13]. The phenomena of multiple phase-separated clusters at steady state is theoretically predicted in bacteria [9], but not in other theoretical models focused on isotropic active particle phase separation[11, 15].

4.4 Cluster growth and coarsening dynamics

It remains an open question in the literature as to how shape may affect the kinetics of phase separation, e.g. coarsening and domain growth laws in active systems. Here, we investigate how particle shape enables the observed phase separation initially into multiple small clusters with coarsening at steady state.

Before phase separating, systems exhibit localized areas of high-density fluctuations, as described in many other theoretical studies of active systems [10, 11]. These localized areas of high density are hexagonally ordered, with the exception of 4-gons, which order on a square lattice. Following this initial structuring, orientational order

develops consistent with the known densest packing of each regular polygon [61]. An example of this phase separation process in vertex-forward 8-gons is shown in Figure 4.3.

This transition from random orientation to close-ordered densest packing is due to the active collision pressure on the clusters. Studies on active disk cluster nucleation have confirmed that inward-pointing particles at the cluster boundary is a necessary condition for nucleation [14, 15]. Similarly, active polygon clusters possess a net-inward force (Figure 4.3a). However, unlike in clusters of disks, the rotation of n-gons within the cluster is sterically inhibited. Thus, there exists a sustained inward-facing pressure on the clusters driving the structure to a densest packing.

We observe that the nature of the phase separation dynamics for shapes resembles that of quenched disks[13] for $n \geq 5$, as seen in Figure 4.1b. Multiple small clusters form and are stable at steady state (where steady state is determined by the methods described in Section 4.2). However, the coarsening behavior between shapes differs. As seen in Fig. 4.1, the critical-regime onset phase separation for $n = [5, 7, 8]$ is characterized by the formation of one (or few) clusters that quickly form and slowly grow, while for $n = 6$, cluster nucleation is so favorable that we see the nucleation of many small clusters even in the critical regime.

We demonstrate this coarsening behavior in Figure 4.8, where the fraction of the system in a cluster (N_C/N) is plotted over time (in units of τ, where τ is the time for a particle to ballistically travel its own diameter). At low densities, but even at those above the critical system density for a given shape, we observe rapid nucleation and growth of small clusters, which remain stable at steady state (this behavior is also observed in the low density/activity limit of dumbbells [29]). At higher densities, the size of the clusters increases the likelihood of another cluster colliding with it and merging to make a larger cluster.

This leads us to another key aspect of anisotropic systems not seen in disks: sus-

tained rotational and translational motion of clusters (Figure 4.9). Previous studies on squares found that sustained motion drove the system into an oscillatory behavior [25]. We find that such motion is also critical to the coarsening of clusters of active shapes. In contrast, clustered disks cannot sustain motion, and quenched systems coarsen through the dissolution of some clusters and growth of others rather than inter-cluster collisions. The only net motion within clusters of disks is at the boundaries, where a balance of particle fluxes in/out characterizes the steady state configuration [13]. As a result, the steady state of multiple small clusters in a system of isotropic particles is unfavorable, as clusters in such systems are only stabilized by particles being self-propelled into the cluster.

4.5 Collision efficiency as a method of quantifying the impact of shape on phase separation behavior

Phase separation due to MIPS is the result of particle slowing as local density increases, with $v(\rho)$ [10]. Here, we demonstrate a method for quantifying the impact of shape on $dv/d\rho$.

To build our intuition for this approach: at a particle level, we can describe MIPS as collision-induced slowing. In a system of frictionless disks, collisions between small numbers of particles are not stable, with clusters of small size ($n_C < 10$) generally having a short lifespan ($< \tau$). (Nucleation in disk systems is facilitated by local polarization of the active force directors leading to a stable nucleation seed [14, 15].) In contrast, collisions between anisotropic particles can create long-lasting clusters of small n_C, "seeds", such as those highlighted in Figure 4.2. In addition to lifetimes lasting $\gg \tau$, some seeds can sustain translational motion and/or stabilize collisions from external particles. While these seeds are not a necessary condition for phase separation, they facilitate the process by slowing both constituent seed particles and

single particles colliding with the seed, leading to localized areas of high density.

At a system level, we can translate this collision-induced slowing to a "collision efficiency" during the nucleation and growth of clusters. We hypothesize that those systems in which collision work is more efficiently transformed into a decrease in average particle velocity (i.e. greater $-dv/d\rho$) are also those that are able to phase separate at lower system densities (lower ϕ^*). As the system density ϕ is a proxy for the number of collisions a particle experiences [16], particles with higher collision efficiency need fewer collisions– and thus lower ϕ– to reduce the average particle speed and lead to phase-separation of the system.

To demonstrate this quantitatively, we measure the instantaneous pressure P_{coll} due to inter-particle collisions (calculations detailed in Section 4.2.3). In Figure 4.10a, we plot the trajectories of systems through v/P_{coll} space. We find that each system type (n and force direction) falls onto a well-defined trajectory with short nucleation, long growth, and flat steady-state regions. The slope of this growth regime, $-dv/d\rho$, is what we term the "collision efficiency". We observe that relative slopes of the growth regimes correctly predict the relative critical densities of the shapes studied, including the relative critical densities of edge-forward and vertex-forward systems of the same shape.

Notably, 3- and 4-gons require significantly higher collision pressure to reach steady state, as shown in Figure 4.10b. These systems fall on the same master curve, suggesting that some feature similarity in the system drives similarity in v/P_{coll} space. Using the concept of collision efficiency, we can now quantitatively demonstrate how the slip planes observed in 3- and 4-gon densest packings lead to the "oscillatory" behavior discussed earlier and observed in previous works [25]. As shown in Figure 4.10c, systems of shapes whose densest packings do not have slip planes (like the edge-forward 5-gons shown) proceed monotonically through v/P_{coll} space with τ, eventually resulting in phase separation. In contrast, systems with slip planes do

not proceed through v/P_{coll} space monotonically with τ. In the system shown of vertex-forward 3-gons, a phase-separating system proceeds through v/P_{coll} space as the phase-separated clusters form. At high P_{coll}, however, the system is no longer able to sustain the inter-particle collision pressure and the cluster breaks apart, retracing its path through v/P_{coll}. Additionally, the lack of hysteresis in this path through v/P_{coll} space during cluster dissolation confirms that this oscillatory phenomenon is not path dependent or a function of simulation protocol, but rather a function of the particle anisotropy alone. The oscillatory regime can be described as a system's inability to stabilize the inter-particle collision pressure.

In collision efficiency, we have introduced a metric that quantitatively explains how shape impacts the critical density in active systems. This framework tells us that we can tune the critical behavior of a system by altering how efficiently particles decelerate other particles in collisions.

4.6 Conclusions

In this work, we investigated the critical phase behavior of a 2D active matter system of anisotropic particles in which anisotropy was implemented through polygon shape and active force director. We demonstrated that we can quantitatively describe the critical behavior as a function of "collision efficiency", which can be tuned by engineering particle interactions (here, we explore only shape). Further, we observe that this critical behavior is related to the structure of the component particle shapes' densest packing at equilibrium.

We showed that increasing the efficiency of inter-particle collisions in slowing particles down during cluster growth is a key driver of decreasing critical densities. This observation is closely related to a number of theoretical developments in the field of active matter. We can think of this efficiency as a determinable scaling coefficient on the change in particle velocity with local density ($dv/d\rho$) in MIPS [9].

Similarly, an analytical determination of the average collision time for an inter-particle collision would allow prediction of critical onset through the balancing of $\tau_{\text{collision}}$ and $\tau_{\text{ballistic}}$ timescales [16]. Such an analytical determination would need to account for all possible angles of collision between anisotropic particles and all iterations of force anisotropy.

An analytical description linking driving force and anisotropy to collision time may enable prediction of critical system densities. Additionally, while the nature of the densest packing in equilibrium can be used to explain the structure seen in dense phase-separated regions, further work is needed to elucidate the link between equilibrium packing and non-equilibrium assembly. As an understanding of the thermodynamics of active matter continues to develop, establishing the phase behavior of active assemblies will be of intense interest as a means of achieving directed, non-equilibrium self-assembly.

While anisotropic active particles are in the early stages of being synthesized in labs they are ubiquitous in nature. Biology presents us with a number of intriguing test cases for our framework– e.g. particle softness, shape irregularity, or non-uniform attraction. How does changing these particle design parameters (as some biological systems are able to do) impact the v/P_{coll} curve? For systems with explicit attractive interactions, e.g. chemotaxis, how can we formulate that interaction as a collision efficiency?

Finally, while our work reveals a mechanism for how particle anisotropy in 2D drives different collective behavior from that seen in disks, our explanation is quantitatively descriptive but not yet analytically predictive of the critical density of a particle shape. Developing a comprehensive predictive theory of how particle anisotropy will impact the critical density would be of great interest to the field.

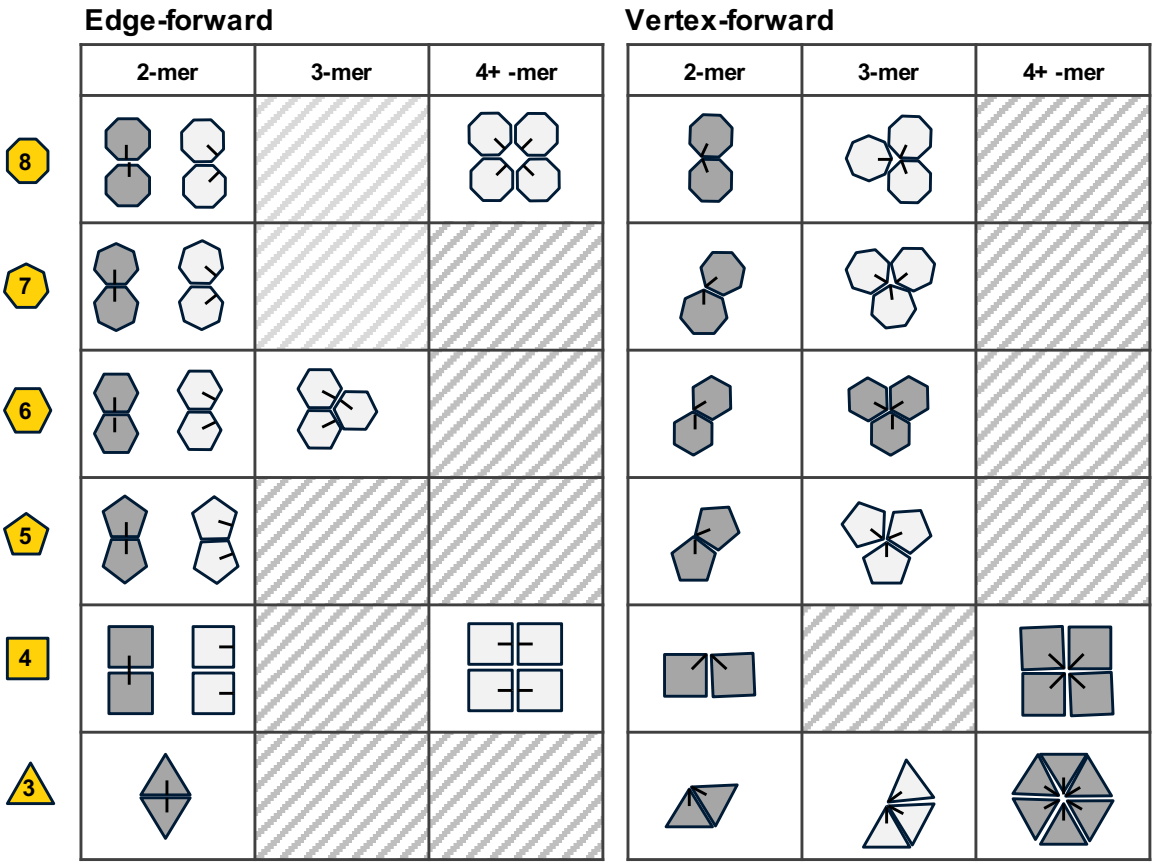

Figure 4.2: Representative clusters are shown for small clusters of all combinations of shape and force director studied. Clusters of shapes in dark grey are those that are commonly observed during cluster formation. Clusters of shapes in light grey are those that can be observed, but are short-lived. Shaded N-mer and shape intersections indicate combinations where there is no stable cluster observed; while it might be possible to theoretically build a cluster of size N for these shapes, we do not see such clusters in practice.

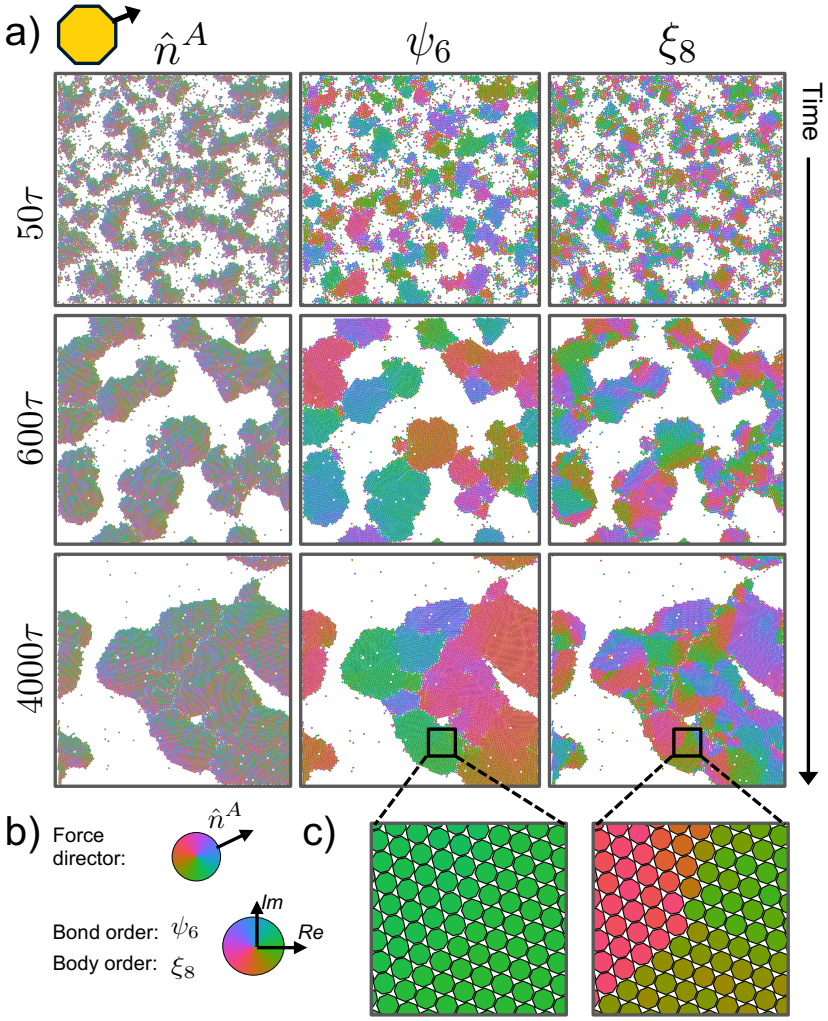

Figure 4.3: Example of structural evolution of clusters in system of vertex-forward 8-gons at $\phi = 0.5$. a) Left column: Active force director $\hat{n}^A$ exhibits strong polarization at all times, pointing towards the center of the cluster both at the boundary and throughout the cluster. Center column: Hexatic bond order ψ_6 forms quickly and uniformly through clusters. Spatial boundaries in the order parameter are the result of cluster mergers that have not yet annealed. Right column: Body order ξ_8 accounts for particle orientation in the cluster. Strong orientational grains form in the clusters, though they do not span clusters as completely as bond order. Grain boundaries are apparent and do not anneal completely. b) Legend for orientation maps in (a). c) Snapshots of bond and body order from regions highlighted in (a).

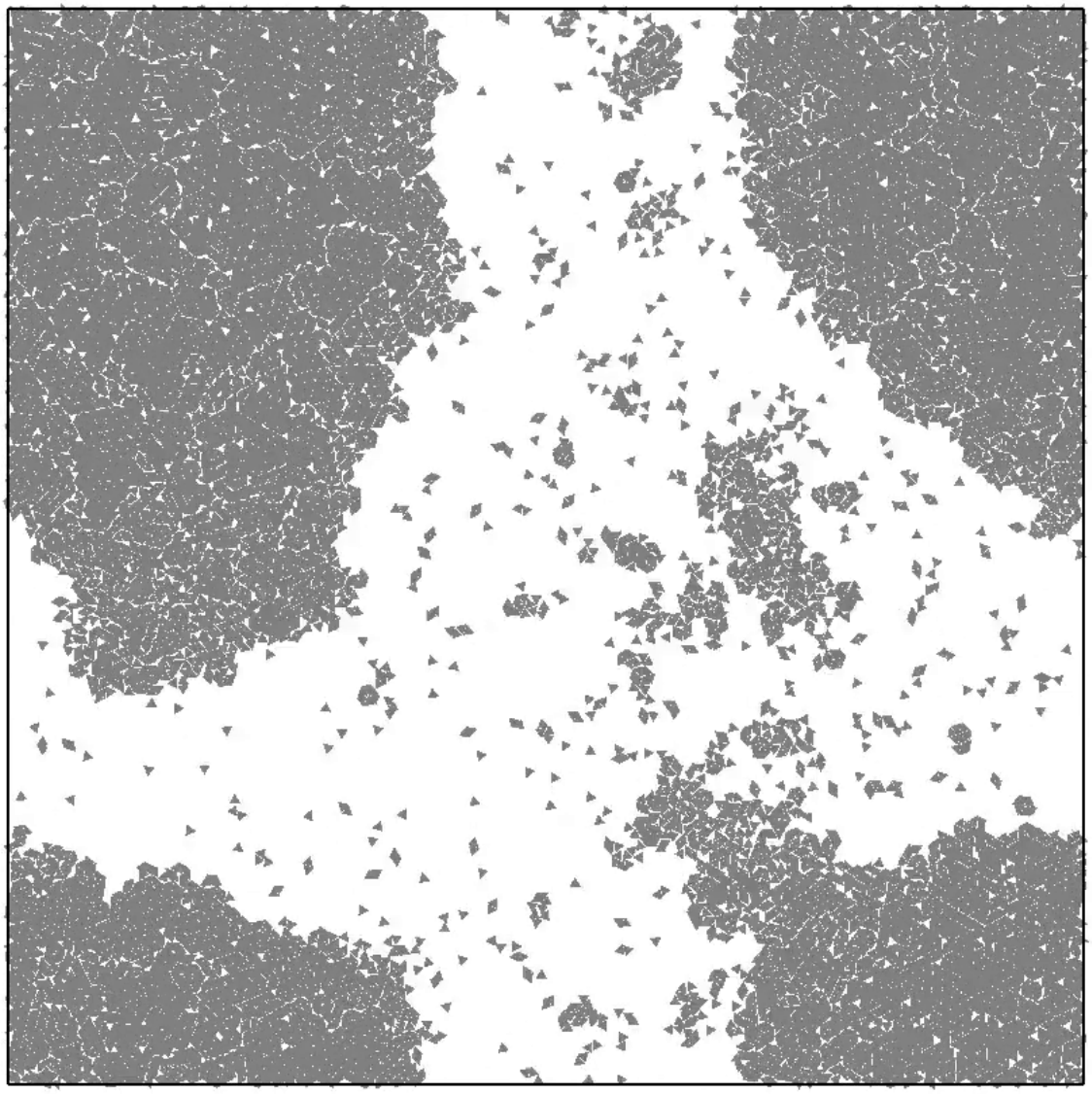

Figure 4.4: Video snapshot: Vertex-forward 3-gons at ϕ=0.50. This video shows the same simulation system whose trajectory is shown in the v/P_{coll} space in Figure 4.10. The system phase separates as the inter-particle collision pressure (P_{coll}) increases. At approximately 3000τ, the system is destabilized as inter-particle pressure builds along slip planes and is released, leading to the break-up of the cluster. This process has been referred to as oscillation in other works. Onset of destabilization is seen at 0:14 in the video. Video file: `n3_VF_phi50.mp4`

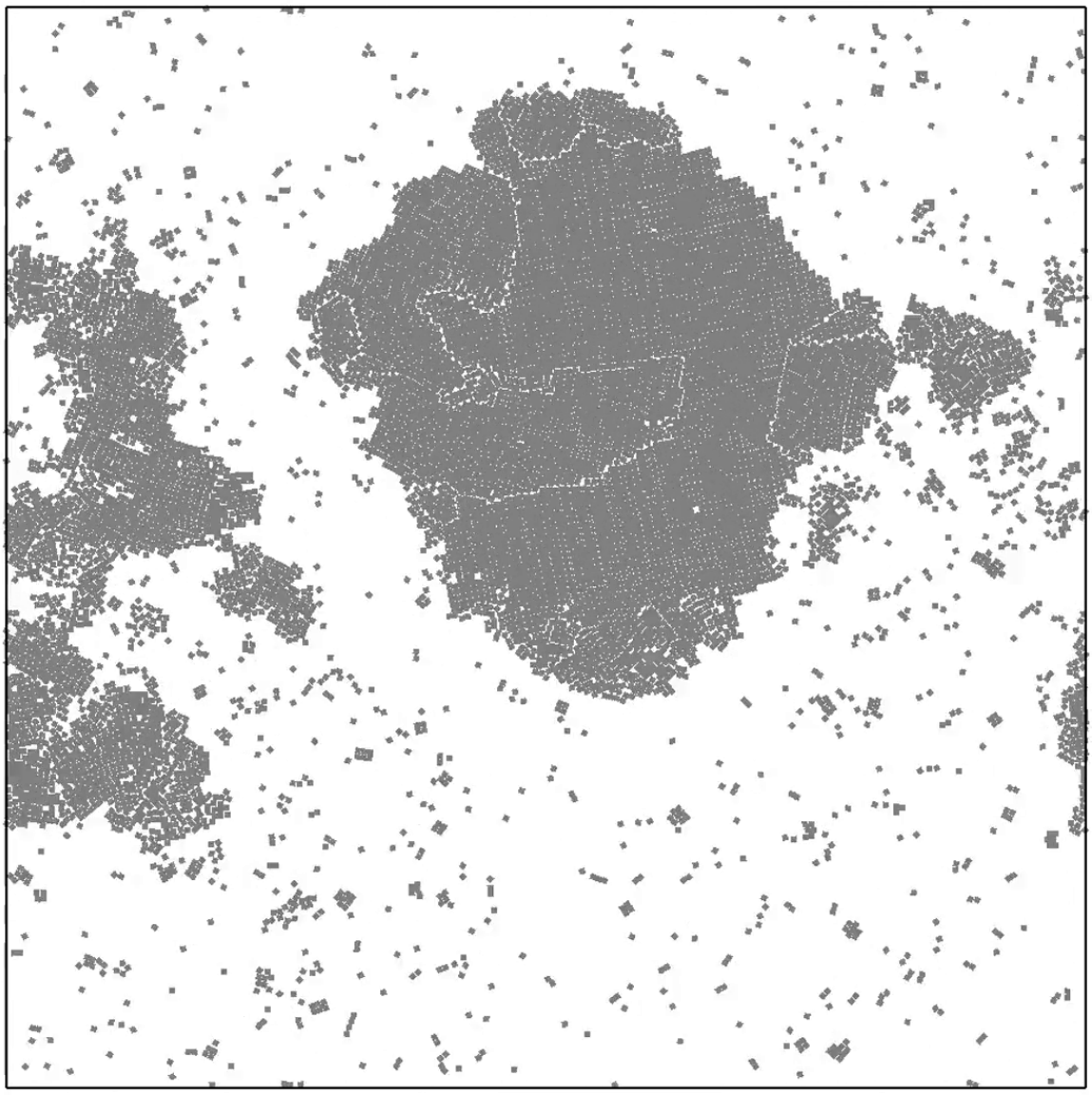

Figure 4.5: Video snapshot: Vertex-forward 4-gons at ϕ=0.50. Clear slip planes are visible in this system that allow the clusters to shear grains off large clusters. This is an example of an "oscillatory" behavior seen in another study of 4-gons. Video file: `n4_VF_phi50.mp4`

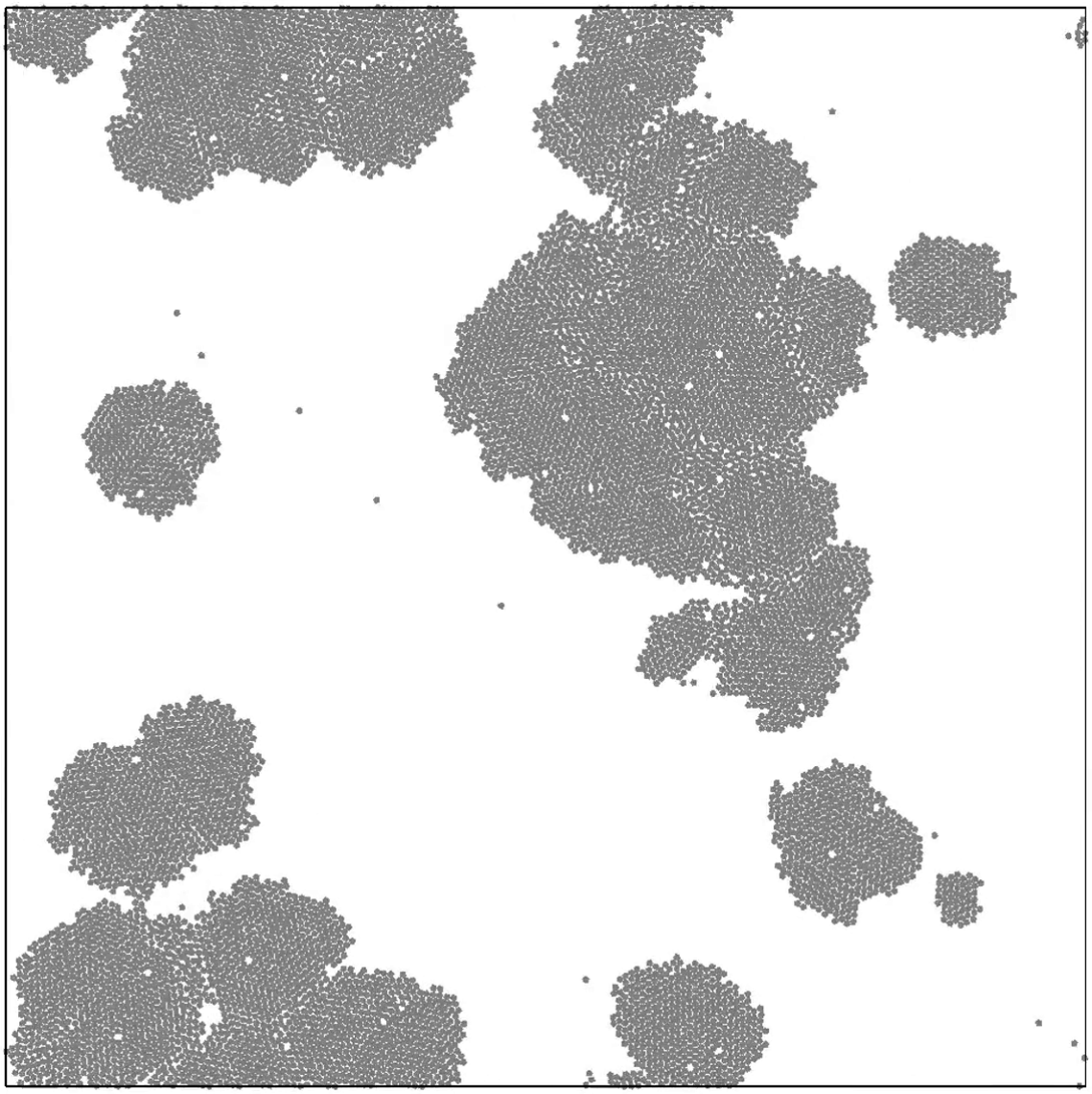

Figure 4.6: Video snapshot: Vertex-forward 5-gons at ϕ=0.50. This system exhibits rapid cluster formation. This system notably phase-separates with a cluster that exhibits the anti-parallel densest packing form common to 5- and 7-gons. Video file: `n5_VF_phi50.mp4`

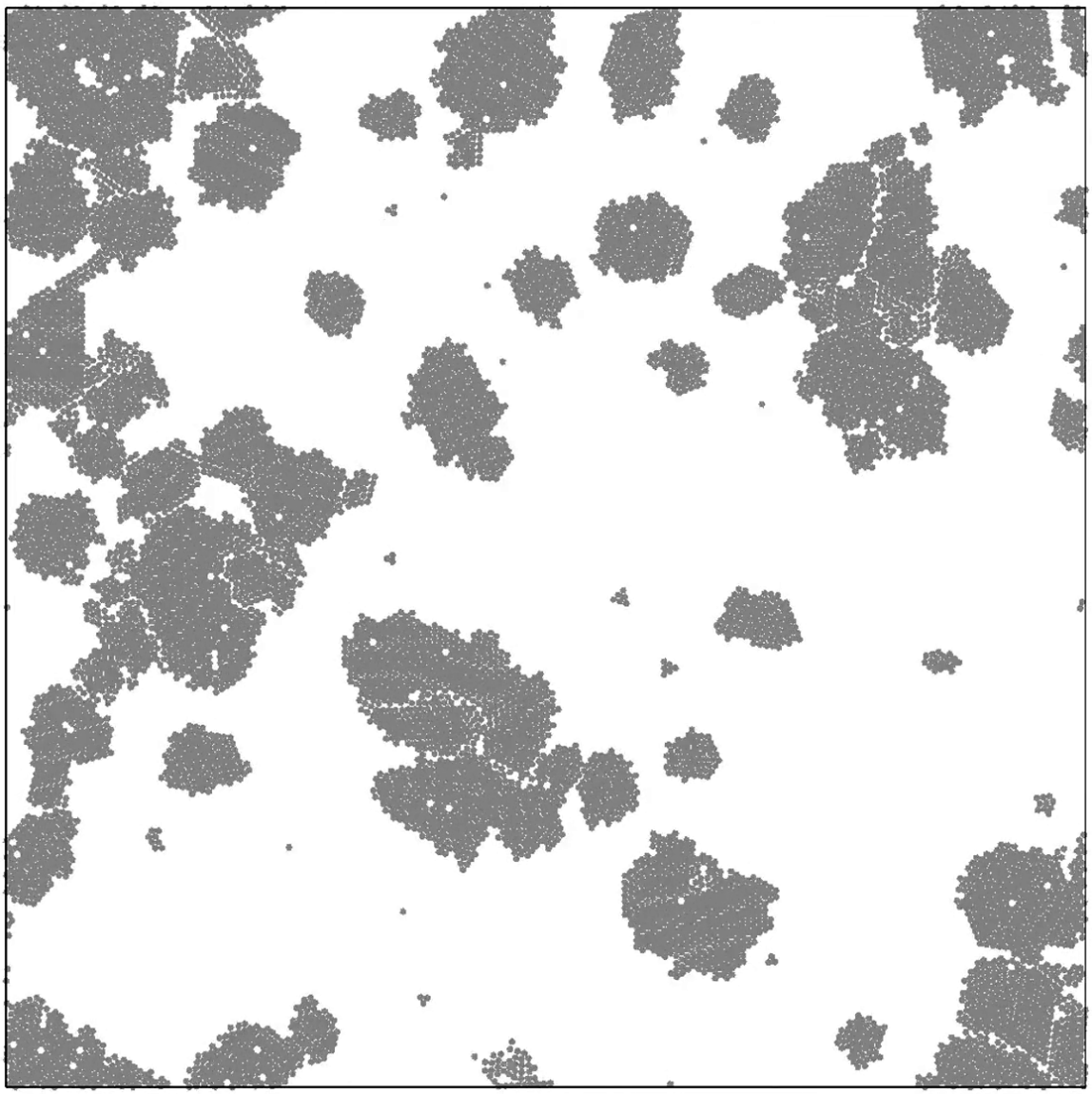

Figure 4.7: Video snapshot: Vertex-forward 6-gons at ϕ=0.50. This system also exhibits rapid cluster formation into many stable, small clusters. Video file: `n6_VF_phi50.mp4`

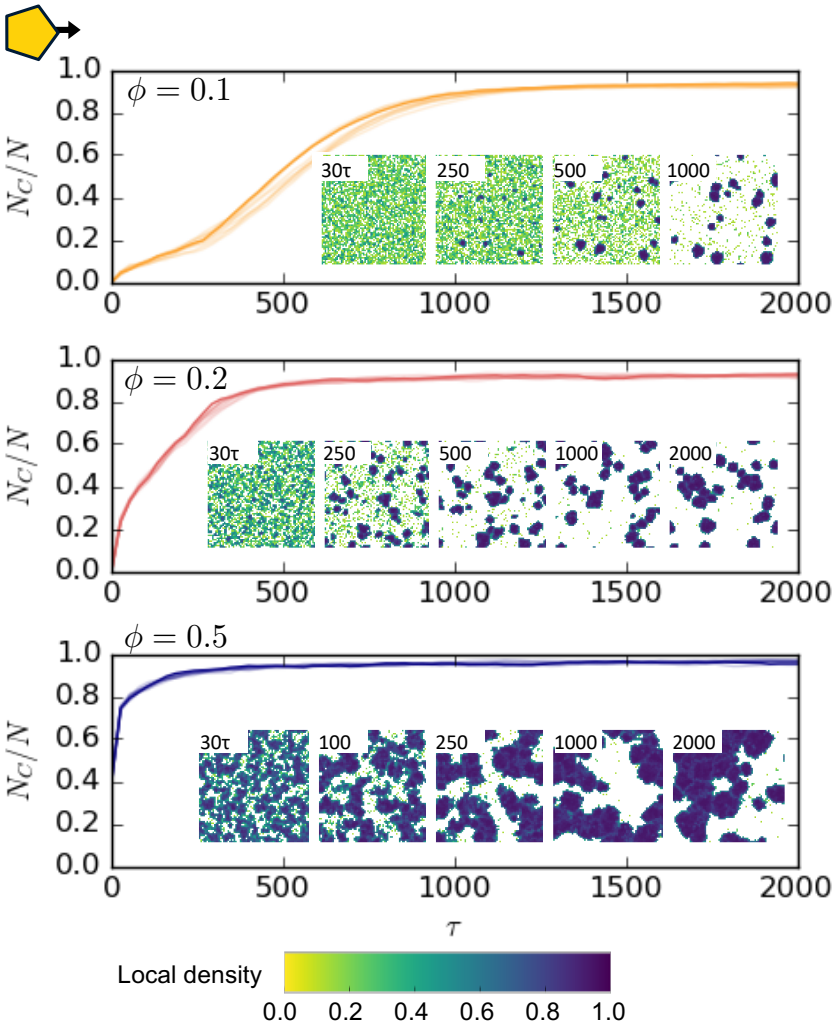

Figure 4.8: Example of phase separation kinetics for vertex-forward 5-gons at three system densities ($\phi > \phi^*$). The fraction of system particles in a cluster, N_C/N, is plotted over the evolution of the simulation. Particles are considered "in a cluster" if their local density is ≥ 0.6. N_c/N trajectories for all ten replicates for each ϕ are shown, though the behavior is so similar that the replicates are only distinguishable for $\phi = 0.1$. Snapshots are colored by local density, colorbar shown.

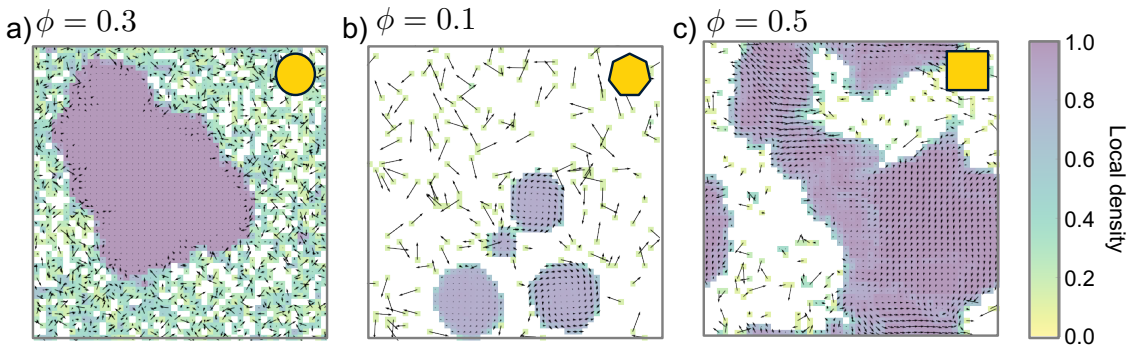

Figure 4.9: Particle displacement fields for simulations at steady state, laid over a map of local densities. (a) Clusters of disks have no net motion, with particle motion limited to the cluster boundaries and gas phase. (Shown is a system of disks at $\phi = 0.3$). In contrast, clusters of anisotropic particles display both (b) net rotational motion (shown for edge-forward 7-gons, $\phi = 0.1$) and (c) net translational motion (shown for vertex-forward 4-gons, $\phi = 0.5$).

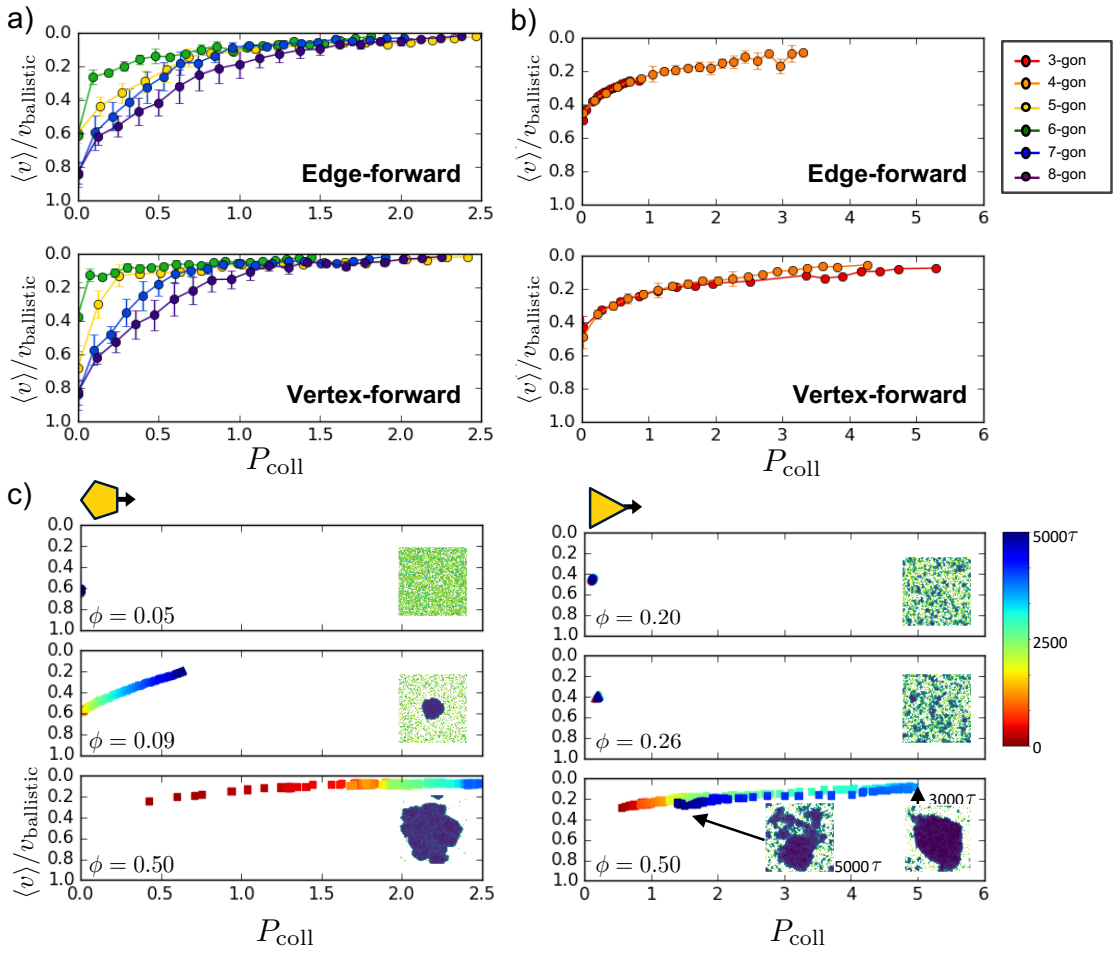

Figure 4.10: (a) Shown are the average trajectories for $5 \leq n \leq 8$ in v/P_{coll} space for both edge- and vertex-forward particle simulations. (Note the inverted axis for velocity.) The nucleation, growth, and steady state regions are highlighted. Increasing slope of the growth regime in v/P_{coll} corresponds to decreased ϕ^*, and is predictive for shapes with given force director. Error bars are the standard deviation, with full calculations detailed in Section 4.2.3. Where error bars are not visible, they are smaller than the data marker. (b) Trajectories for 3- and 4-gons are plotted separately. Here, both shapes collapse onto one master curve. The master curves for edge- and vertex-forward 3- and 4-gons also collapse onto on another. Error bars are calculated as in (a). (c) Individual trajectories are shown for 5- and 3-gons at the indicated ϕ. While velocity decreases monotonically with increasing P_{coll} for 5-gons, in 3-gons we observe an "oscillation" in which the largest cluster in the system breaks up at $\phi = 0.50$. Pressure and velocity snapshots are taken every 100τ.

CHAPTER V

Shape-driven Effective Interactions Access Novel Emergent Behavior in an Active Binary System

This chapter is adopted from a manuscript in preparation with co-author Sharon C. Glotzer.

5.1 Introduction

Studies of self-propelled active particle systems have demonstrated that particle shape can change the emergent and critical behavior of a system through steric-induced changes to particle collisions. This raises the question: how would multiple steric-induced collision types in a system impact the observed collective behavior? Here, we computationally explore the emergent behavior found in binary mixtures of self-propelled polygons at different stoichiometry. We find emergent phenomena that, to our knowledge, has not been seen in other systems of active matter. First, we identify microphase separation resulting from "steric bonding", a shape- and activity-induced preferential attraction we can quantify between like species in the absence of explicit attractive interactions. Second, we observe the formation of stable fluid clusters at steady state, resulting from the addition of a second shape type that disrupts the dense-packing formation of the first shape type. This structural disruption and

corresponding increase in particle motility also facilitates the formation of a larger phase-separated regime. Finally, we highlight that the same mechanism that enables fluid clusters can also stabilize a three-phase steady state with a fluid cluster, solid cluster, and sparse gas phase. Importantly, all the observed behavior is sensitive to chosen design parameters (stoichiometry). That we find such rich phenomena in investigating just a narrow slice of the design space for self-propelled active particles highlights the potential for a wide range of engineered behavior in such systems.

5.2 Analysis methods

5.2.1 Choice of systems

We use the particle implementations described previously to study these systems (see Chapter III). Here we study regular polygons of side number $3 \leq n \leq 8$. In Chapter IV, we found that the critical density of systems of active polygons for 5 sides and above did not strongly depend on the direction of the force director. For this study, then, we set the force director to be fixed to the particle shape propelling the shape vertex-forward. In the previous Chapter, this was shown to lead to lower critical densities for 3- and 4-gons than an edge-forward configuration.

We fix all systems studied here to a packing fraction of 25%. Systems studied are all two-component systems of $N = 1 \times 10^4$ particles. The stoichiometry of components in the system ranges from 10/90 to 90/10, and are as specified with the corresponding results.

For comparison, we also studied systems where both component shapes have equal side length. In such systems, we set all component shapes to have a standard side length equal to that of a 6-gon of $\zeta = 9$, while keeping $r_{WCA} = 1$ (see Section 3.1 for definitions). Importantly, this means that these shapes no longer have the same rounding (ζ). However, the constant r_{WCA} helps ensure a consistent penetration

length for the excluded volume potential.

5.2.2 Calculating the cluster size distribution

The cluster size distribution is given by the number of clusters (n_s) of size s/N, where s is the number of particles in the cluster and N is the number of particles in the system. We sample at every 100 time units (τ, the time it takes a particle to ballistically travel its own diameter) at the steady-state configurations of each simulation, and calculate error bars over all samples from all replicates.

5.2.3 Calculation of steric attraction

Bond homophily: Bond homophily is the preference for like-like neighbor pairing of a given particle type, normalized to what would be predicted by the stoichiometry of the system. As an example, in a two component system with 50%/50% stoichiometry, if species A's neighbors are on average 55% species A and 45% species B, the bond homophily of species A will be $\frac{55\%}{50\%} - 1 = +10\%$. Using this same example, we see that the prior statement regarding species A's bond homophily does not give us explicit information about species B's bond homophily. Species B's homophily can only be calculated by looking at the neighbors of species B on average.

Nearest neighbors were identified using the Cluster module of the analysis package Freud `2.1.0` [55]. Neighbor lists were calculated using the Freud package's implementation of an Axis-Aligned Bounding Box (AABB) tree [65], with a ball query with maximum radius equal to $2.5x$ the circumscribing radius of the largest shape and self-exclusion. This choice of maximum radius is sufficient to capture the first neighbor peak in our systems.

Calculations were done on the final frame of each simulation over all particles in the system that had at least one other neighbor. This was done to capture steady-state bond preferences.

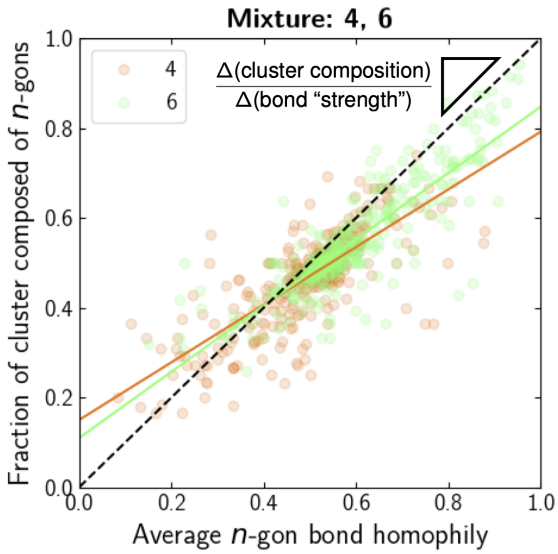

Figure 5.1: Example of the underlying data used to calculate steric attraction, shown here for 50/50 mixture of 4- and 6-gons. Each point represents data for one cluster, over which the bond homophily and cluster composition are averaged. The trend line is a linear regression best fit for each particle type. The dashed line has a slope of 1, and indicates a hypothetical system where each increase in bond homophily corresponds to an exact increase in cluster composition

Strength of steric attraction: We define the "strength of steric attraction" as:

$$\text{Strength of steric attraction} = \frac{\Delta(\text{cluster composition})}{\Delta(\text{bond homophily})} \tag{5.1}$$

Cluster composition is the fraction of each cluster that belongs to each particle type in the two-component systems studied here. We calculate the cluster composition and bond homophily at 10 snapshots for each simulation, at timepoints ranging from 10τ to 5000τ (the final frame). We only considered clusters with at least 10 particles in the calculations.

For each particle type, for each cluster, we can then plot the cluster's composition versus the average bond homophily for the given particle type in that given cluster. Over all simulations for a given component mix, we can then calculate a best-fit line whose slope is the impact of each incremental increase in particle type bond homophily

on the cluster composition. This slope is the "steric attraction" for a given species. A sample system is shown in Figure 5.1. The standard error of the estimate for each calculated slope is calculated as $\sigma_{\text{est}} = \sqrt{\frac{\sum(Y-Y')^2}{N}}$ where Y is the actual value (in this case of cluster composition), Y' is the predicted value, and N is the number of data points.

In theory, the maximum of the slope of these linear fits should be 1. A slope of 1 indicates that each increase in bond homophily corresponds to a direct increase in the cluster composition. We might expect to see this in systems with complete species separation.

5.2.4 Cluster lifetime calculations

To calculate the cluster lifetime for systems of varying stoichiometry of 3-gons, we calculate the percentage of original cluster particles at time t_0 that are still in the cluster at t_1. Sampling begins after the system has reached steady state, and samples are taken every 50τ with 500τ between t_0 and t_1. The resulting value for the fraction of particles still in the cluster is calculated over all samples, over all replicates. The error bars are given by the standard deviation over this same sample.

5.3 Emergent behavior diagram

In combining multiple components into the same system, we might expect to see particles de-mix and separate into large like-like clusters [23, 27]. Additionally, from our previous work in one-component systems (Chapter IV), we know that shapes pack into their equilibrium densest structure in the phase separated cluster, and that the structure of the densest packing can be used to explain their phase separation behavior. Given this, we expected that mixtures of particles of shapes with incommensurate densest packing structures might de-mix completely.

Instead, we see the varied emergent behavior summarized in Figures 5.2 and 5.3.

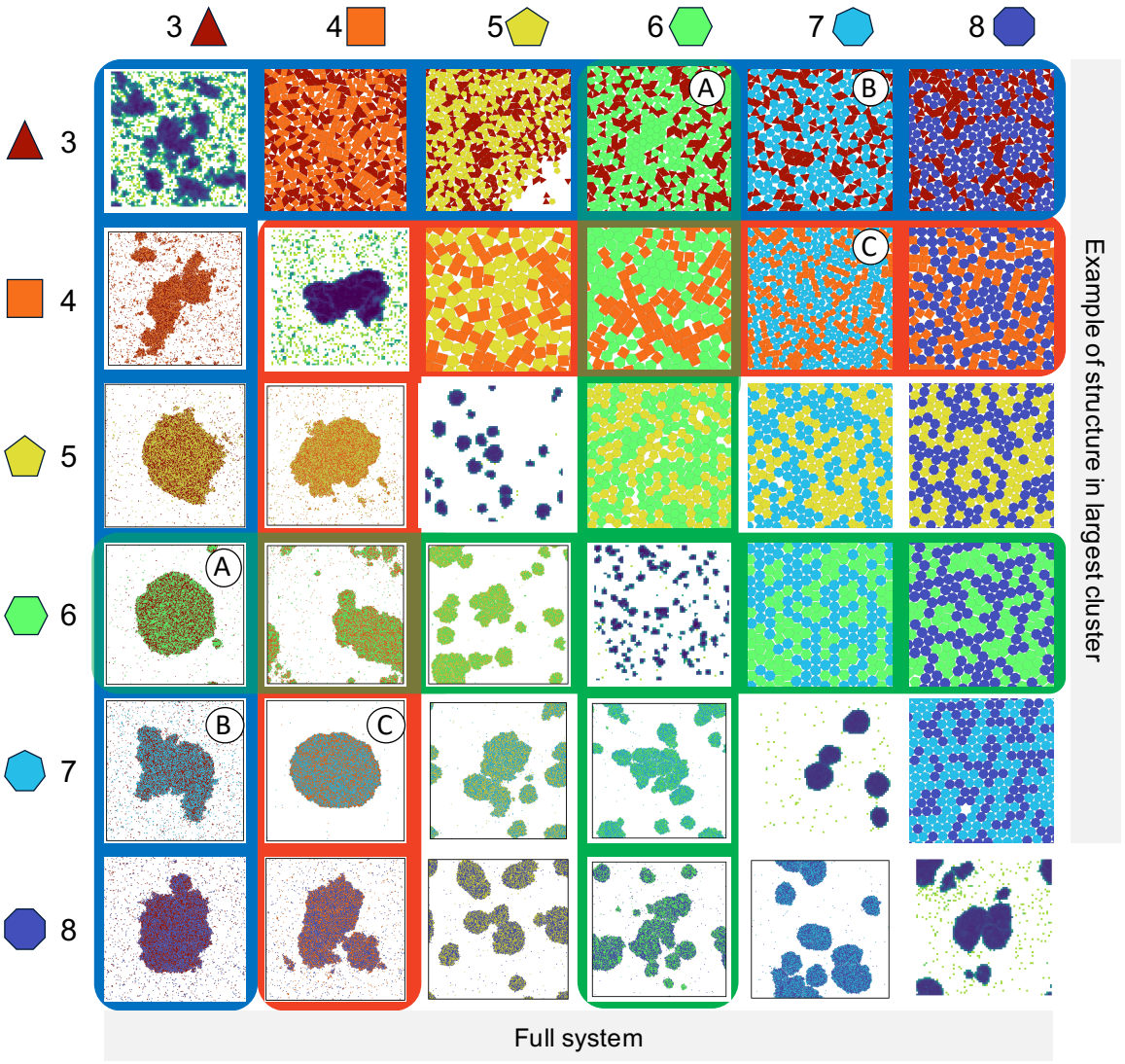

Figure 5.2: Shown are data for simulations at 50/50 stoichiometry. Full system snapshots (lower triangle) and snapshots of dense cluster structure (upper triangle) at each binary mixture studied. On the diagonal are the one-component systems, shown above their respective critical densities and colored by local density. The systems exhibiting the novel behavior discussed in this work are highlighted as follows. Green: Microphase separation. Blue: Fluidizer behavior. Red: Three-phase steady-state. Snapshots A, B, and C are highlighted in Figure 5.3.

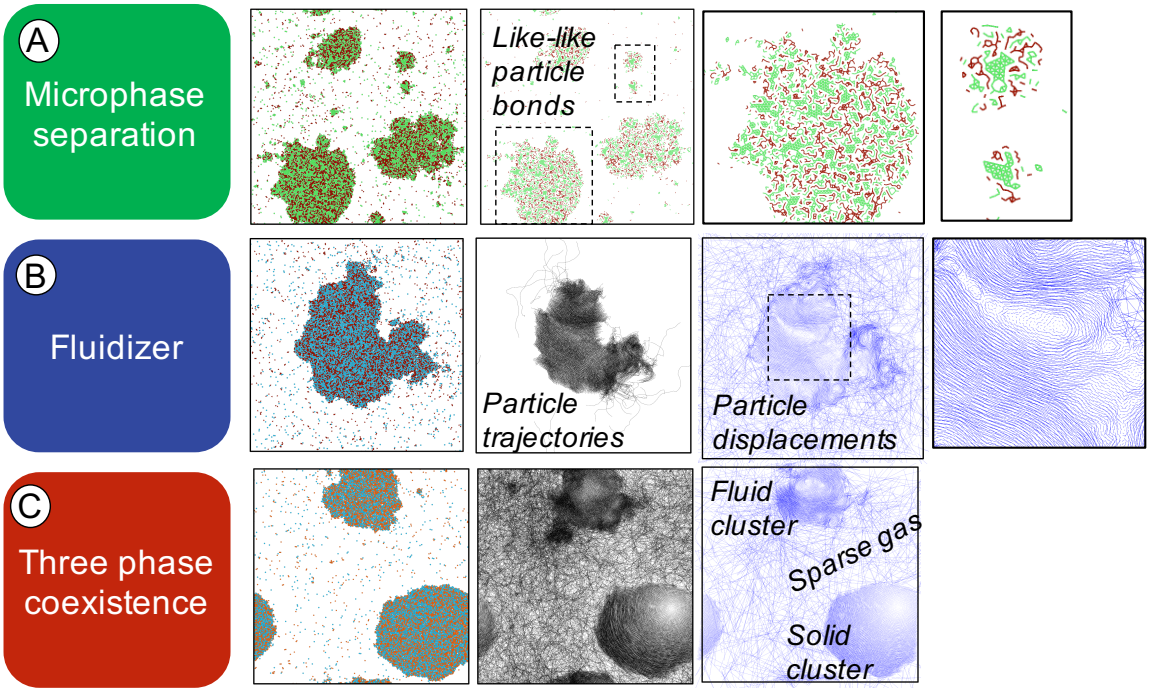

Figure 5.3: Examples for each of the three behaviors highlighted in this work. A snapshot of each representative system is shown at steady state at left. All systems shown are at 50/50 stoichiometry. A) Microphase behavior in 4/6-gon mixture. Like-like bonds are shown in the same particle colors as the keys in Figure 5.2, highlighting that 6-gons form compact clusters within a mixed cluster. Zoomed-in snapshots are on right. B) Fluidizer behavior in 3/7-gon mixture. Maps of both particle trajectories and displacement highlight the internal motion in the stable cluster. C) Three-phase steady-state in 4/7-gon mixtures. As with the fluidizer behavior, particle trajectories highlight a fluid cluster, but also demonstrate that the second large cluster is a solid, with both clusters existing in a third sparse gas phase.

We find three new-to-active-matter behaviors: microphases in systems with 6-gons, stable fluid clusters with 3-gons, and a three-phase steady-state accessible in systems with 4-gons.

Why might we be seeing such behavior? We again turn to the structure of the phase-separated cluster for clues. In systems with 3- and 4-gons, we note that the edge length difference between particles leads to more compact grains of 3- and 4-gons, with less compact grains of their partner shapes. We know that these shapes have shear planes in their densest packings which lead to oscillatory phases in one-component systems (Chapter IV). We posit that even the disperse grains of these particles lead to similar behavior in multi-component systems, destabilizing the larger cluster while its partner particles prevent the cluster from dissolving fully, and discuss this further in Section 5.5.

At the other end of the structural similarity spectrum, we see systems of combinations of 5-, 7-, and 8-gons pack into a well-mixed packing that resembles that of disks. While like shapes still approximate their densest packing structure when with a like neighbor, on the macroscale the behavior seems to be largely shape-agnostic.

At the macroscale, we also observe that the appearance of the phase separated cluster changes in some systems. For systems of $n \geq 5$, steady state is characterized by multiple stable clusters. However, upon the addition of 3- or 4-gons, steady-state in the phase separation regime is instead characterized by one to two large clusters. This provides a hint at the mechanism for phase separation into a fluid cluster: in addition to shear along slip planes, fluid clusters may also be the result of multiple potential clusters coexisting in one dense phase. We will explore this further in Section 5.6.

Finally, we see what we term "microphase separation" of 6-gons forming [relatively] large grains within phase separated clusters, seen clearly in Figure 5.3. We emphasize that we mean "microphase" in the more traditional sense of separation of species within the same phase in multi-component polymer systems, rather than

recent work looking at phase separation of one-component active matter into "micro" phase separated regimes[66].

Videos of all three phenomena are found in Video Figures 5.4, 5.5, and 5.6.

5.4 Microphase separation stems from shape-driven effective attraction

Classical microphase separation is mediated by preferential attraction between species [67]. In the systems studied here, particles have no explicit attraction interaction and only interact via excluded volume interactions. However, we know that in equilibrium excluded volume interactions can lead to effective entropic "bonding" through such interactions[68]. While the concept of equilibrium entropy-driven behavior does not map neatly onto active matter systems, we can ask if a similar shape-mediated "attraction" is seen in active systems.

We approach this two ways. First, we look at the micro-scale impact of particle shape on inter-particle interaction preferences. In Figure 5.7a, we measure the preference of a particle type to bond with itself in a mixture with other particle types. Interestingly, we find that some shapes have a *negative* bond preference versus stoichiometry, indicating that such systems are more well-mixed at the microscale level than stoichiometry would suggest. Such systems are combinations of 5-, 7-, and 8-gons– the same systems highlighted in Section 5.3 as packing like disks.

Next, we see that 6-gons strongly prefer neighbors of their own type when in mixtures of any other particle, up to 7% (when in combination with 8-gons) above what would be predicted based on stoichiometry (e.g. in a system with 50/50 stoichiometry, 50% of particle bonds would be expected to be like-like versus like-unlike). Interestingly, this same preferential bonding extends to the other species in the mixture with 6-gons, and we confirm this behavior is consistent when particles are resized to have

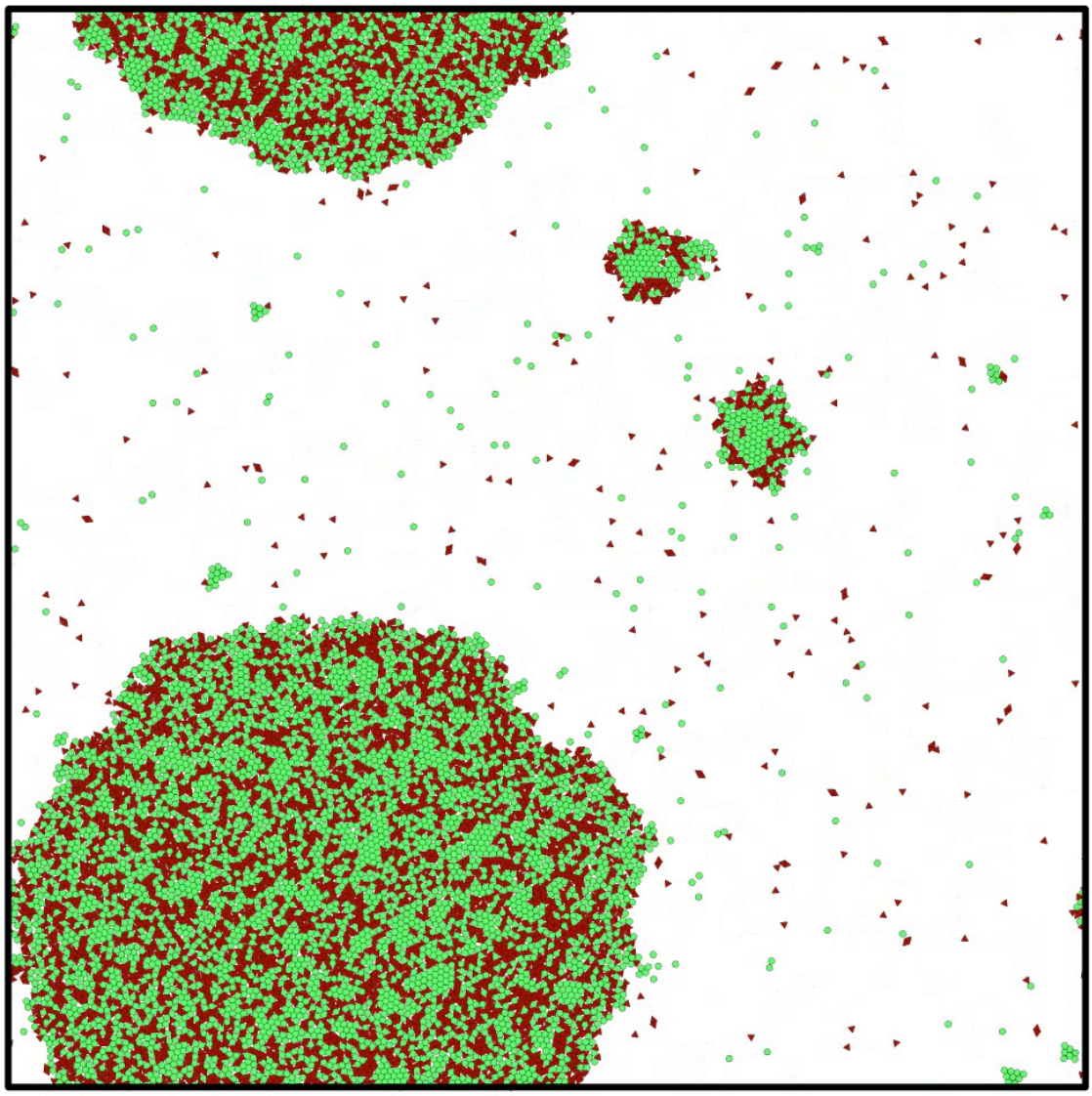

Figure 5.4: Video of 4- and 6-gons at 50/50 stoichiometry (screenshot shown, file: `microphase_separation.mp4`). Full phase separation process is shown, including significant time at steady state. Particles are colored as in Figure 5.2.

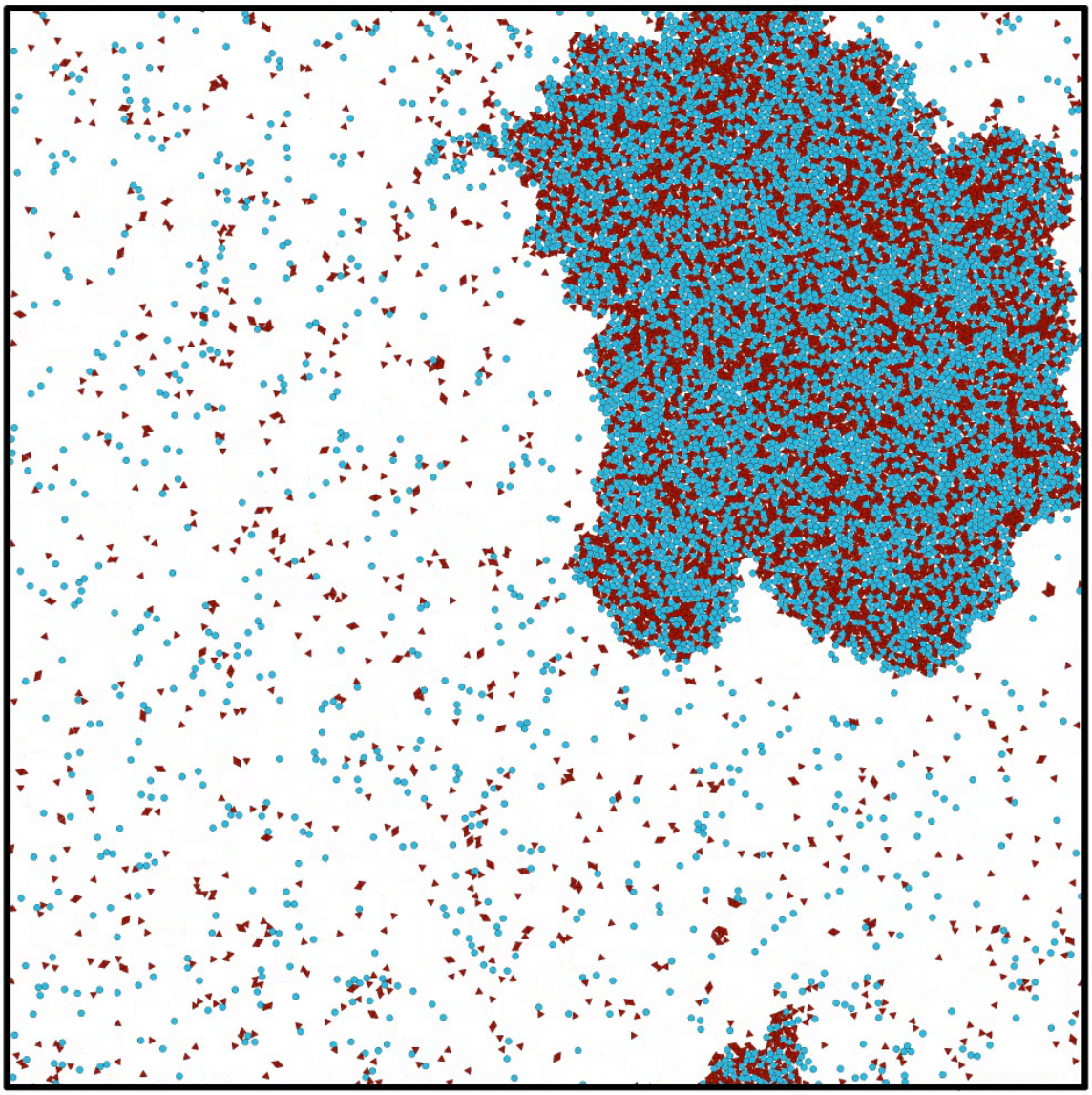

Figure 5.5: Video of 3- and 7-gons at 50/50 stoichiometry (screenshot shown, file: `fluid_cluster.mp4`). Full phase separation process is shown, including significant time at steady state. Particles are colored as in Figure 5.2.

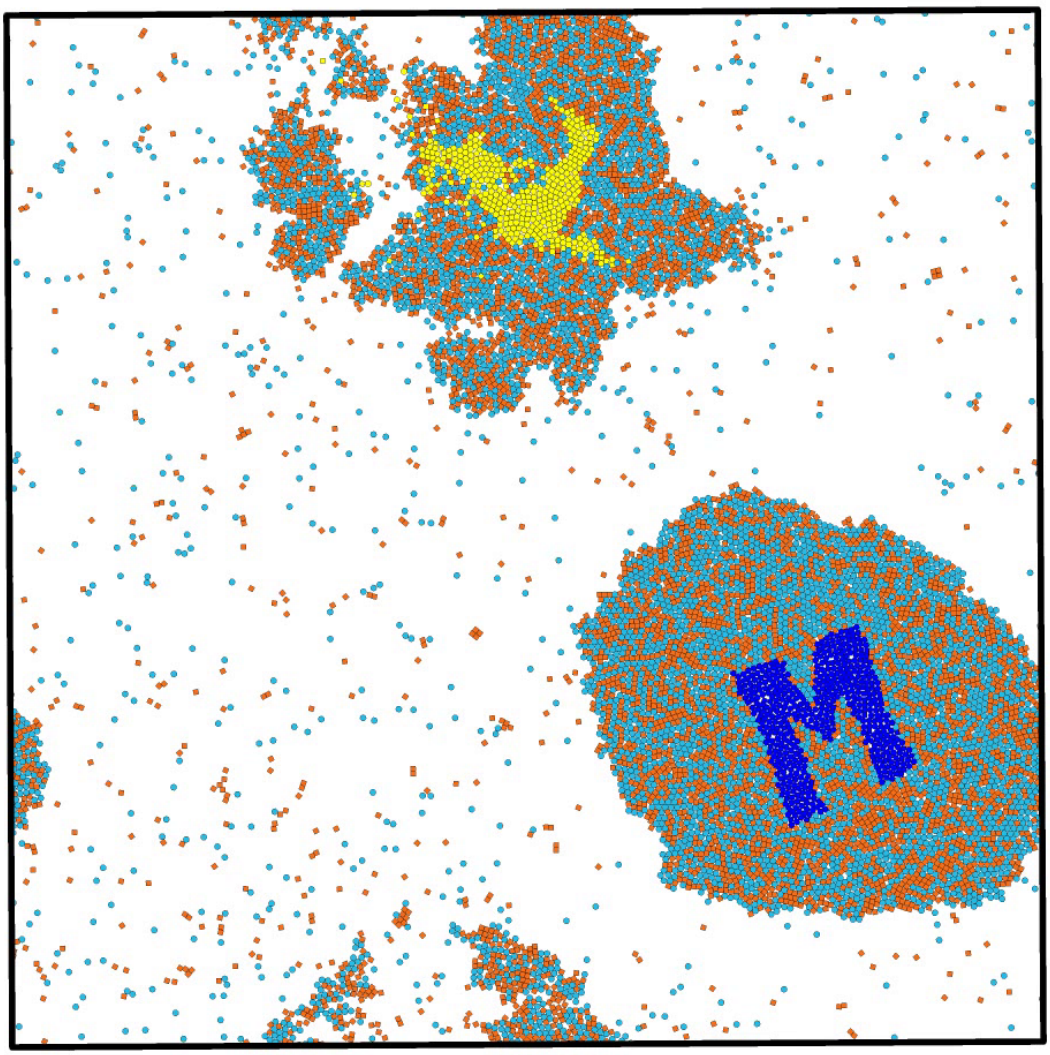

Figure 5.6: Video of 4- and 7-gons at 50/50 stoichiometry (screenshot shown, file: `three_phase_coexistence.mp4`). This video is truncated to the same period as shown in Figure 5.11. Particles are colored as in Figure 5.2, excepting the representative "U" and "M" to highlight in-cluster particle movement.

equal side lengths. This suggests that 6-gons are uniquely able to drive steric preferences at the micro-scale. However, phase separation, including microphase separation, is typically seen on the macroscale.

To quantify the system-scale impact of particle shape, we look at the macro-scale impact of particle shape interaction preferences on the composition of their resident clusters. We can define a "strength of steric attraction" as $\frac{\Delta(\text{cluster composition})}{\Delta(\text{bond preferences})}$, with full calculation details in Section 5.2.3. For a given cluster, we can measure the bond preference of each species and the overall composition of the species. Over all clusters, we can then calculate the change (Δ) we see in cluster composition with changes in bond preference.

We see in Figure 5.7b that 6-gons, in all possible system compositions, exhibit the strongest steric bonding. That is to say, they are most effectively able to convert microscale "bonding" preferences to macroscale cluster composition preferences. In bond preferences, we see that 6-gons are able to effect bond preferences in their system partner; however, we do not see 6-gons affecting the *steric attraction* of their system partners. This difference further suggests that there is something different about the 6-gon particle "bonds". Since the bonding preference for all other n-gons when paired with 6-gons is likely 6-gon-mediated, that bonding preference is insufficient to drive macro cluster preferences on its own.

We can see an example of what this macro/micro-preference difference looks like in Figure 5.8. Using a binary system of 4- and 6-gons as an example, we see a strong peak in the pair correlation function ($g(r)$, Figure 5.8b) for 6-6 self-bonds and a nearest-neighbor peak more than 50% smaller for 4-4 self-bonds, with a wider tail due to 4-gons' ability to pack into an offset "subway tiling" (see Figure 5.8 inset). These large peaks corresponded to face-to-face packing between like particles, as would be predicted in equilibrium through entropic bonding theory[68, 69]. Likewise, the first peak in the smaller 4-6 bond correlation function corresponds to the face-

to-face contact between a 4- and 6-gon. The pair correlation function highlights two important findings. First, that particles have clear preferential self-binding that is also found in the structure of the cluster. Second, that this self preference corresponds with a preference for face-face interaction.

In Figure 5.8c, we take a macro view of the system and see that the self-cluster size distributions for each shape in the system collapse onto one another. For both shapes in the system, their distribution of the size of like-like clusters is the same. If we predicted that bond strength would also correspond to the size of grains of like particles, this is not what we would expect. This perhaps suggests a limit to the impact steric interactions can have on macroscale behavior, and is seen in all systems studied (see Figure 5.9). Actively "annealing" such systems, e.g. cycling the active force, would be an interesting approach to exploring if this limit is a true property of such systems.

5.5 Fluidizing is driven by increased motility in clusters with 3-gons

As it's clear from Section 5.4 that triangles do not have any specific negative steric binding interactions, we investigate whether they "fluidize" clusters in some other way.

A key clue, as previously discussed, comes from the fact that we observe more consolidated clusters of particles of size $n \geq 5$ when in systems with 3-gons than when in one-component systems. In addition, one-component 3-gon systems exhibit an oscillatory phase where clusters dissolve along slip plans in the densest packing. Might these be related?

We investigate this by calculating the cluster lifetime of clusters of 3-gons and other particle types at varying stoichiometry. We find that generally, an increasing

percentage of 3-gons in the systems leads to shorter cluster lifetimes. This may seem counter-intuitive, as we just stated that these fluid clusters are in fact larger and more stable than clusters found at steady state in either of their component's respective one-component systems. However, if we think of 3-gons as the destabilizing force in a cluster, leading to motion, and their mixture partner as the cluster-stabilizing component, one can imagine that a balance of these two forces might lead to shorter-lived small clusters with force-balanced larger, longer-lived clusters.

As we will see in the next section, fluid clusters form from combinations of smaller clusters, lending further support to this idea that movement within and between small clusters as part of a whole is critical for a stable fluid cluster phase.

5.6 Three-phase steady state highlights delicate balance of structural stability in clusters

Finally, we highlight that the same fluid clusters found in systems with 3-gons can also be found in systems with 4-gons– another shape with slip planes in its densest packing. In this case, we observe that such clusters can coexist with a sparse gas phase and solid cluster, as shown in Figure 5.11.

An important question is: why do some clusters become fluid, but others solid? In Figure 5.12, we follow the evolution of the three-phase system explored quantitatively above and find that the fluid cluster forms through early, multi-cluster combinations, while solid clusters form through incremental addition to a solid cluster "seed". Such formation is also not uncommon in one-component systems. What sets these two-component systems apart is that, like discussed in Section 5.5, there is a balance between one component's destabilization of the cluster (3-, 4-gons), and their system pair's stabilization of a solid cluster. Thus, that we get both fluid and solid clusters possible in such two-component systems is a product of balancing possible structural

stabilities after random initialization.

There does not appear to be a meaningful difference in the stoichiometry or particle bond preferences between the two different cluster types.

5.7 Conclusions

In this work, we started by investigating binary systems of self-propelled polygons in equal stoichiometric ratios. We observed three new-to-active-matter phenomena: microphase separation, fluidizer-like behavior, and a three-phase steady state. Our work here highlights the richness– and the wide space of unknowns– in designing active matter systems with novel and specific emergent phenomena.

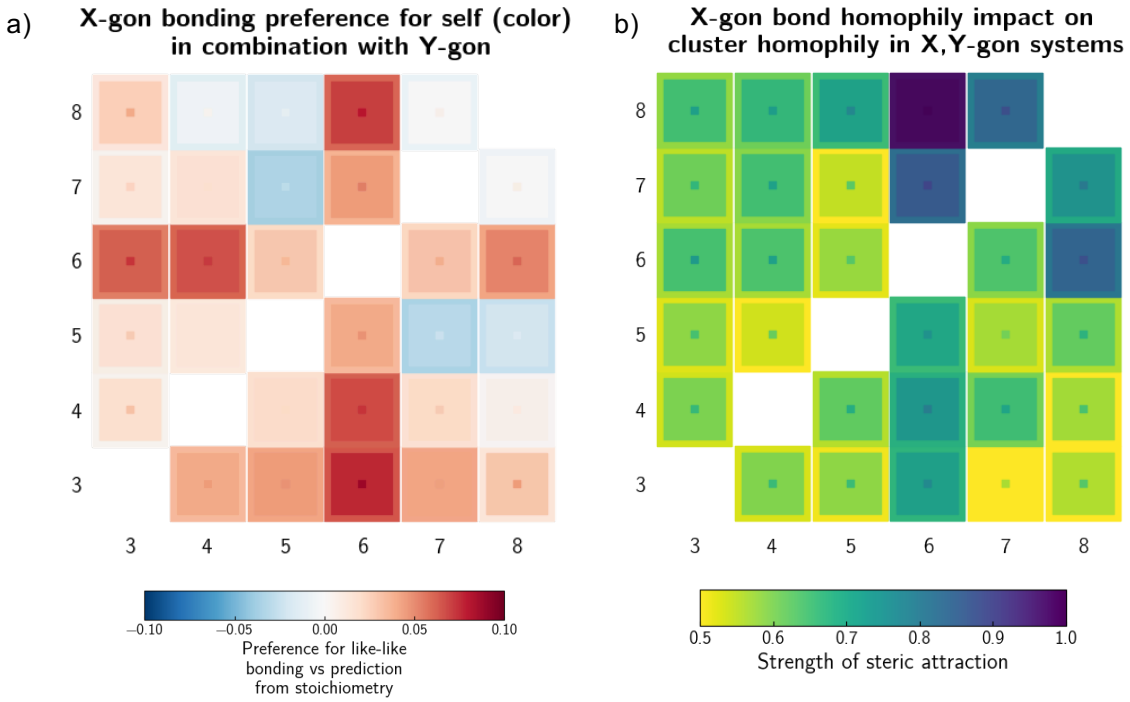

Figure 5.7: Quantification of shape-driven effective interactions in mixtures. a) Preference for like-like bonding versus prediction from stoichiometry. Higher values indicate a higher likelihood of nearest neighbors being like particles, versus the prediction from stoichiometry. Error for each intersection is shown as the outer ring (lower bound of the standard deviation) and inner dot (upper bound of the standard deviation) of each square. b) Degree to which like-like bond preference drives increased like-particle cluster composition. The hypothetical upper value is 1.0, in which every fractional increase in like-like bond preference leads to a corresponding increase in the composition of a cluster that is like particles. The hypothetical lower bound should be the stoichiometry of the system, in this case 0.5 for both particles. As in (a), the error for each intersection is shown as the outer ring (upper bound of the standard error of the estimate) and inner dot (upper bound of the standard error of the estimate) colors. We do not necessarily expect these plots to be symmetric.

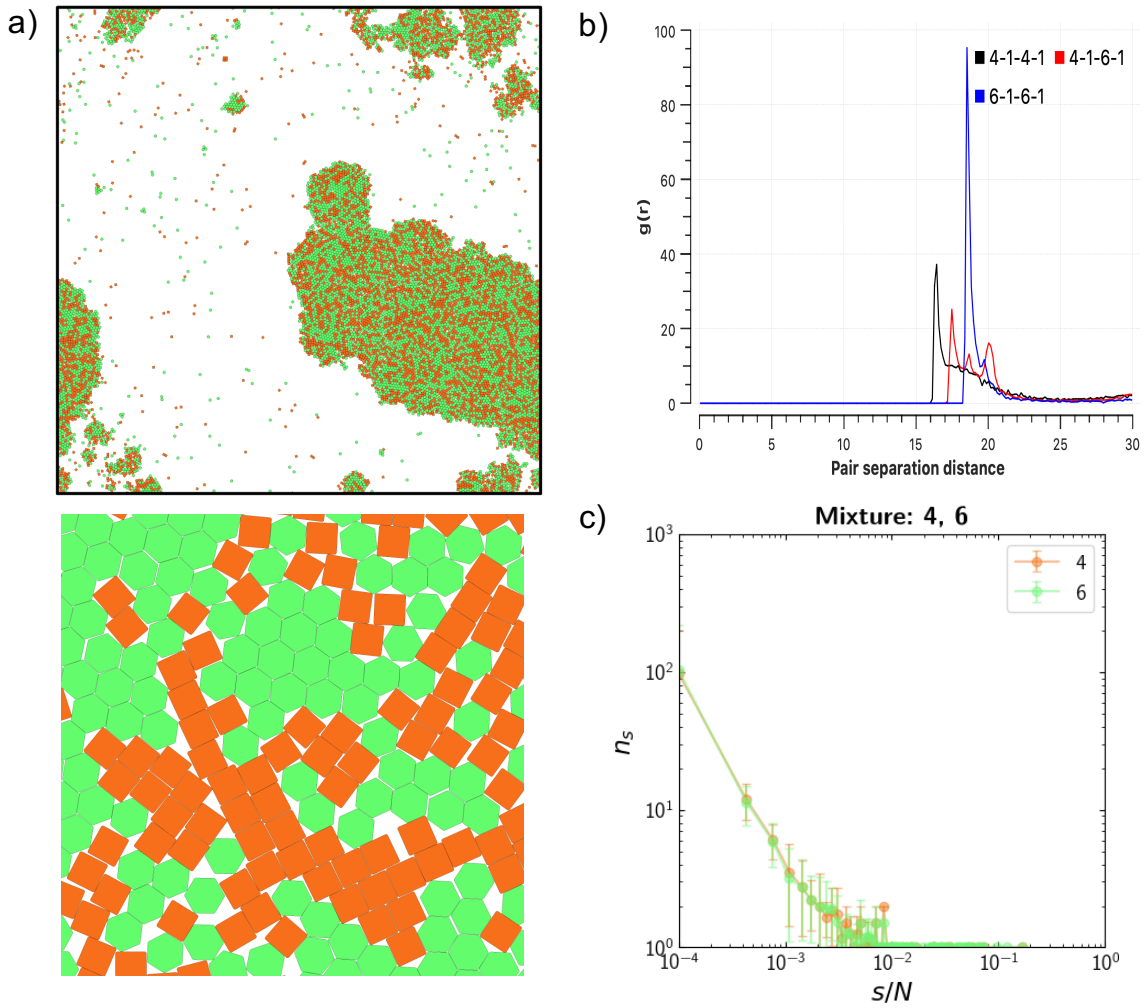

Figure 5.8: a) Snapshots of a 50/50 mixture of 4- (orange) and 6-gons (green) at steady state. The bottom is a snapshot of the structure in the phase-separated cluster. b) Pair correlation $g(r)$ between all species in the mixture, with pair colored per the legend. c) Cluster size distribution, as calculated in Section 5.2.2.

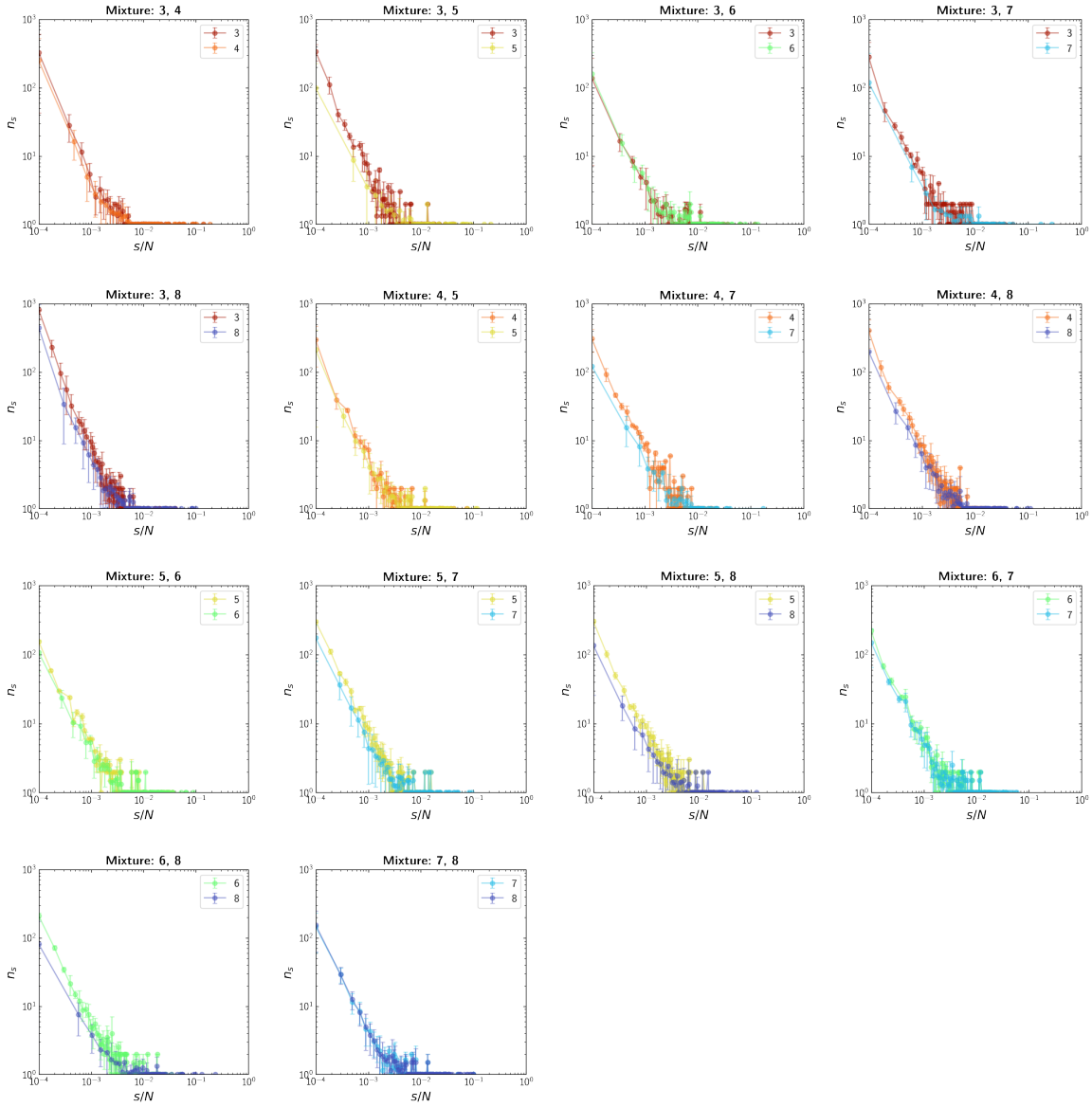

Figure 5.9: Cluster size distributions for all systems under study, as calculated in Section 5.2.2. We note that the curves collapse for all systems shown.

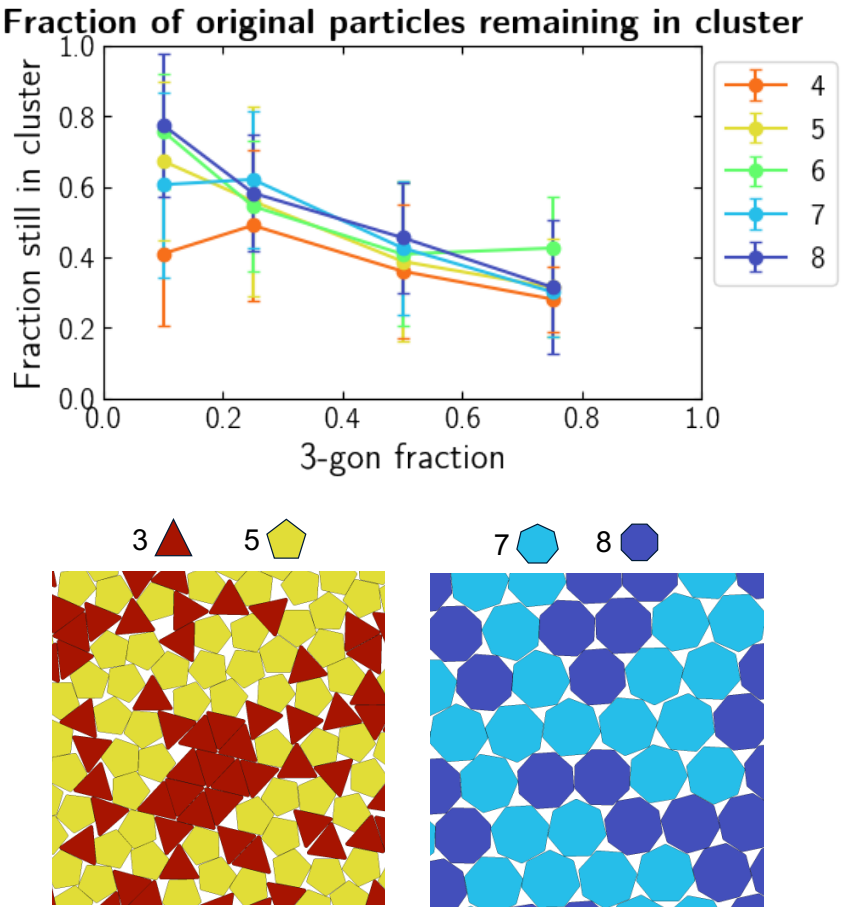

Figure 5.10: Top: The fraction of original particles from time t_0 still in a cluster at t_1 is used as a proxy for the average cluster lifetime. We see that higher fractions of 3-gons in a system lead to shorter cluster lifetimes. Bottom: We highlight one possible explanation for this: the structure of 3-gons and other particle types are incommensurate when not at an equal side length.

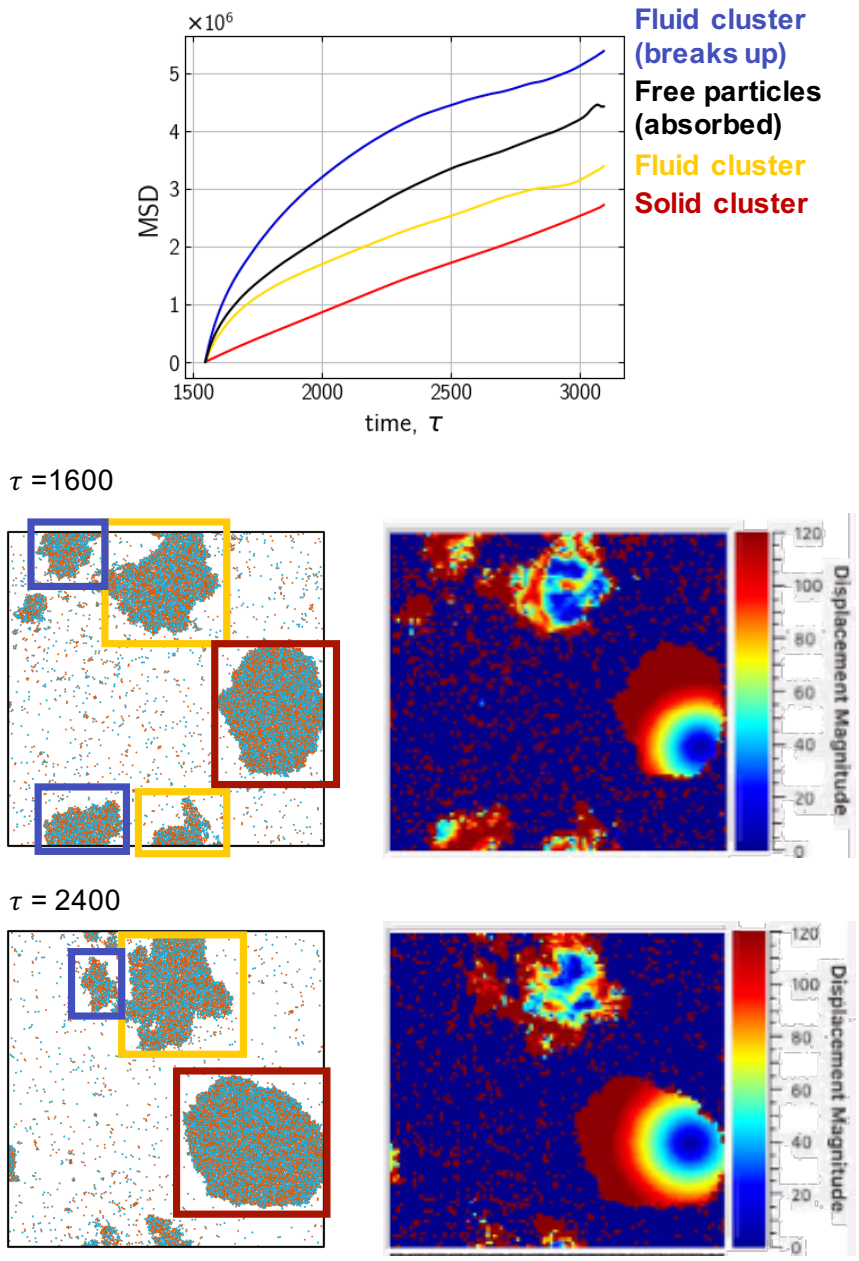

Figure 5.11: We observe coexisting gas, fluid, and solid phases in an example three-phase steady state system of 4- and 5-gons in a 50/50 stoichiometry. In the bottom snapshot, clusters are highlighted in the color corresponding to their color in the plot of mean square displacements at top. All particles in clusters of size less than 10 are included in the "Free particles" MSD calculation. In addition to the MSD, which plots displacement over time, instantaneous displacement snapshots are shown to the right of the system snapshots at bottom, as calculated by Ovito[2].

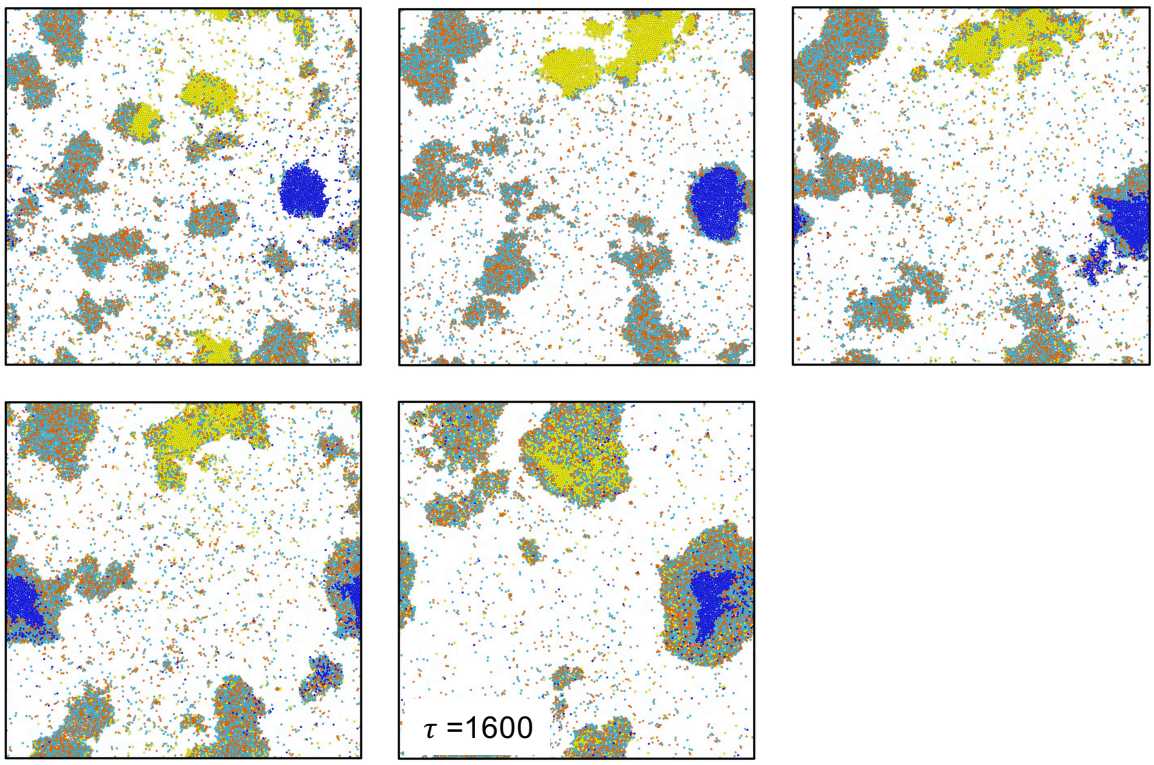

Figure 5.12: Snapshots of the system shown in Figure 5.11 evolving to steady state, with time increasing from upper left and concluding at the first frame of Figure 5.11 calculations. A sample of particles destined for the fluid cluster are shown in yellow, and a sample of particles destined for the solid cluster are shown in blue. We see that as the clusters forming the fluid cluster collide, there is significant mixing at the boundaries and sustained continued motion. In contrast, while the sample of particles destined for the solid cluster deforms slightly, it forms the basis of the solid cluster as additional particles are added through incremental addition, rather than large-scale cluster addition.

CHAPTER VI

Particle Shape Leads to Different Universal Behavior in Active Systems

This chapter is adopted from a manuscript in preparation with co-authors Robert Ziff and Sharon C. Glotzer.

6.1 Introduction

Active matter phase separation is a non-equilibrium phase transition with no clear equilibrium counterpart, as phase separation occurs even in the absence of explicit attractive forces. Recent efforts have sought to map the simplest active matter system, isotropic active Brownian particles, onto equilibrium universality classes as means of extending active matter theory. Given the significant impact even implicit steric interactions can have on the phase separation behavior in such systems, we pose the question: are changes to the effective interactions between active Brownian particles due to steric interactions (shape) sufficient to change the universality class of an active matter system? We propose a mapping of active matter near the order-disorder transition onto a non-equilibrium directed percolation model. In doing so, we are able to identify distinct curve collapses of cluster formation in the 2D active polygon systems studied here. We further explore the critical behavior of these groups and

find that the quasicritical behavior of the cluster scaling distribution predicts the same groups as our curve collapses. Further work will be needed to confirm the critical exponents, including a more rigorous finite size scaling approach to identify the critical point of each system.

6.2 Background

Active matter phase separation is a non-equilibrium phase transition with no clear equilibrium counterpart, as active Brownian particles undergo phase separation into coexisting sparse and dense regions in the absence of explicit interactions [4, 5]. As discussed in Chapter II, changes to the particle design of such active Brownian particles can effect changes to the phase separation onset parameters and emergent behavior (e.g. swarming, arrested phase separation, clustering), even without the addition of explicit attraction rules.

One potential approach to a theoretical framework of the impact of inter-particle interactions on the system is to map the system onto a known universality class. Identifying universal behavior allows us to transfer knowledge of a well-studied system to a different, less well-characterized system.

Previously, work in this area has focused on mapping onto an equilibrium system and investigating the non-equilibrium effects on the system's critical behavior. Previous studies have mapped the active Ising model[70] and a lattice model of active Brownian particles [71] onto the equilibrium Ising universality class. Separately, studies of the phase transition in a non-lattice system of active Brownian particles demonstrated that system did *not* demonstrate scaling behavior of the equilibrium Ising universality class[72]. That a mapping of active matter onto an equilibrium phase transition could be sensitive to such a difference in system configuration highlights that changes to the active Brownian particle interactions are likely to lead to changes in the phase transition behavior and, perhaps, changes in universal scaling

behavior.

We propose a slightly different approach than those taken previously: can we map an active Brownian particle phase transition onto a well-studied class of *non-equilibrium* phase transitions? Such an approach has previously been used to identify an anisotropic percolation transition in the Vicsek model with explicit interaction terms[73]. We investigate whether changes to implicit interactions via shape are sufficient to drive systems of different particle shape types into different universality classes– and if so, whether they are classes new to active matter or well-known non-equilibrium universality classes.

We expect the potential for multiple universality classes for two reasons.

First, the impact of particle shape anisotropy on system phase separation and emergent behavior has been found to be highly shape-specific (e.g. Chapter IV and V). Second, we can extend findings from percolation in which different local bond rules lead to different universality classes. One of the simplest non-equilibrium universality classes, directed percolation, describes systems in which the probability of a bond forming is not uniform in all directions. However, changes to the local rules governing bond formation in a non-equilibrium percolation model can lead to networks with different universality classes [74]. Extending the analogy to active matter, we might expect that changes to "local rules"– e.g. changing the steric interactions between particles due to shape– might lead to different universality classes as well.

6.3 Analysis methods

6.3.1 Normalizing time to account for noise in active systems

In a non-equilibrium process with noise, systems originating from different random configurations do not phase separate at a uniform absolute time. Typically, phase separation requires some "nucleation"-type event to facilitate the onset of clustering.

We use a normalized time $\theta/\theta_{\text{free}}$ to account for the likelihood of these nucleation events with changes to shape, system density, and active force.

Here, θ is the time it takes for a given particle to ballistically travel its own diameter, and is only a function of shape and the active driving force. To account for differences in the system densities (which correspond to the likelihood of "nucleation"-inducing collisions), we calculate the time for a particle to travel the mean free path, θ_{free}. From the classic collision theory of reaction kinetics, we can describe the mean free path (λ) as

$$\lambda = \frac{v_0 t}{(2d)(v_0 t)\Phi} = \frac{1}{(2d)\Phi} \tag{6.1}$$

where v_0 (particle speed) and t (time) cancel out to leave λ a function only of the shape cross-section, d, and system density, Φ. The time for a particle to travel this mean free path, then, is:

$$\theta_{\text{free}} = \frac{\lambda}{v_0} = \left(\frac{1}{(2d)\Phi}\right)\left(\frac{1}{v_0}\right) = \frac{1}{2d\Phi v_0} \tag{6.2}$$

We set $\theta/\theta_{\text{free}}$ equal to zero at the point the cluster fraction $N_{\text{clustered}}/N > 0.5$. The final time to plot is determined by the time at which the cluster fraction reaches 0.95.

6.4 Mapping continuum active matter behavior with steric interactions onto a percolation model

We map active systems with shape-induced steric interactions onto a percolation-like model as outlined in Table 6.1.

However, a key element that we do not have is that of a spanning cluster. In percolation models, the percolating cluster is one that spans the simulation box from edge to edge. Instead, we calculate whether the system has phase separated or not, based on the calculations laid out in Section 4.2.1.

Value	**Percolation**	**Active systems**	
Bond/site occupancy probability	p	Φ	Probability of a "bond" occurring
System size	N or L	N	Number of components in a system that could be connected through an event occurring with probability p/Φ
Largest cluster fraction	C/N	C/N, $N_{\text{clustered}}/N$	Largest cluster remains the same; however, as some systems phase-separate very quickly, $N_{\text{clustered}}/N$ can also be a proxy
Normalized time / progress	t/N	$\theta/\theta_{\text{free}}$	Time, normalized to the system's settings

Table 6.1: Mapping of percolation quantities to active matter system quantities.

Given what may seem to be a fundamental difference between percolation and the active systems under study here, a natural question might be: why map this onto percolation at all? We do this in part because other studies have successfully identified percolation transitions in active systems [73], and in part because directed percolation is the simplest non-equilibrium universality class we could envision a mapping to [3]. Additionally, as discussed earlier the local preferential bonding rules of non-equilibrium percolation models provide a simple analogy for the preferential steric attraction and "bonding" seen in shapes. This mapping provides a useful framework for evaluating the critical behavior of active shape systems, if not a perfect match.

6.5 Phase separation behavior

While in the thermodynamic limit $P(\Phi)$ is a step function with the jump exactly located at the phase transition, in finite systems $P(\Phi)$ is smoothed around the finite-

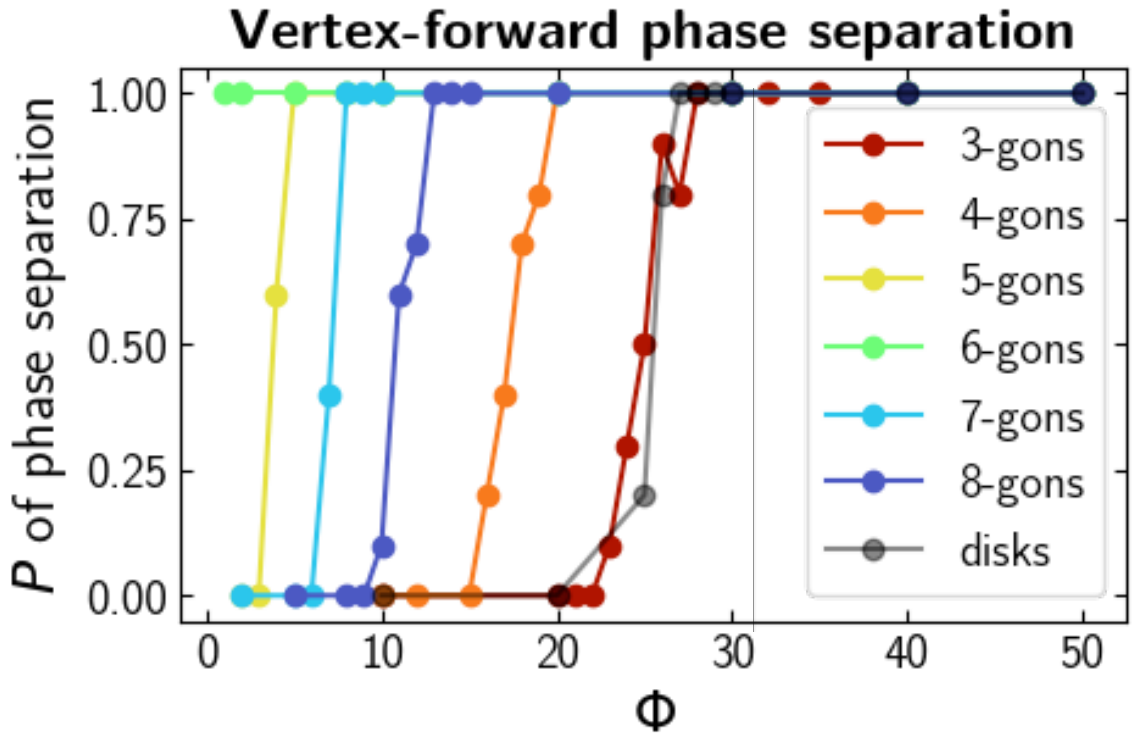

Figure 6.1: Probability of phase separation occurring in systems of varying shape anisotropy. Probability is calculated as the fraction of replicates at each parameter combination (Pe=150, and density as indicated) that phase separate for systems of 10,000 particles. This closely resembles $P(\rho)/\rho$ plots for calculating the probability of a percolating cluster over varying system densities (e.g. [3]).

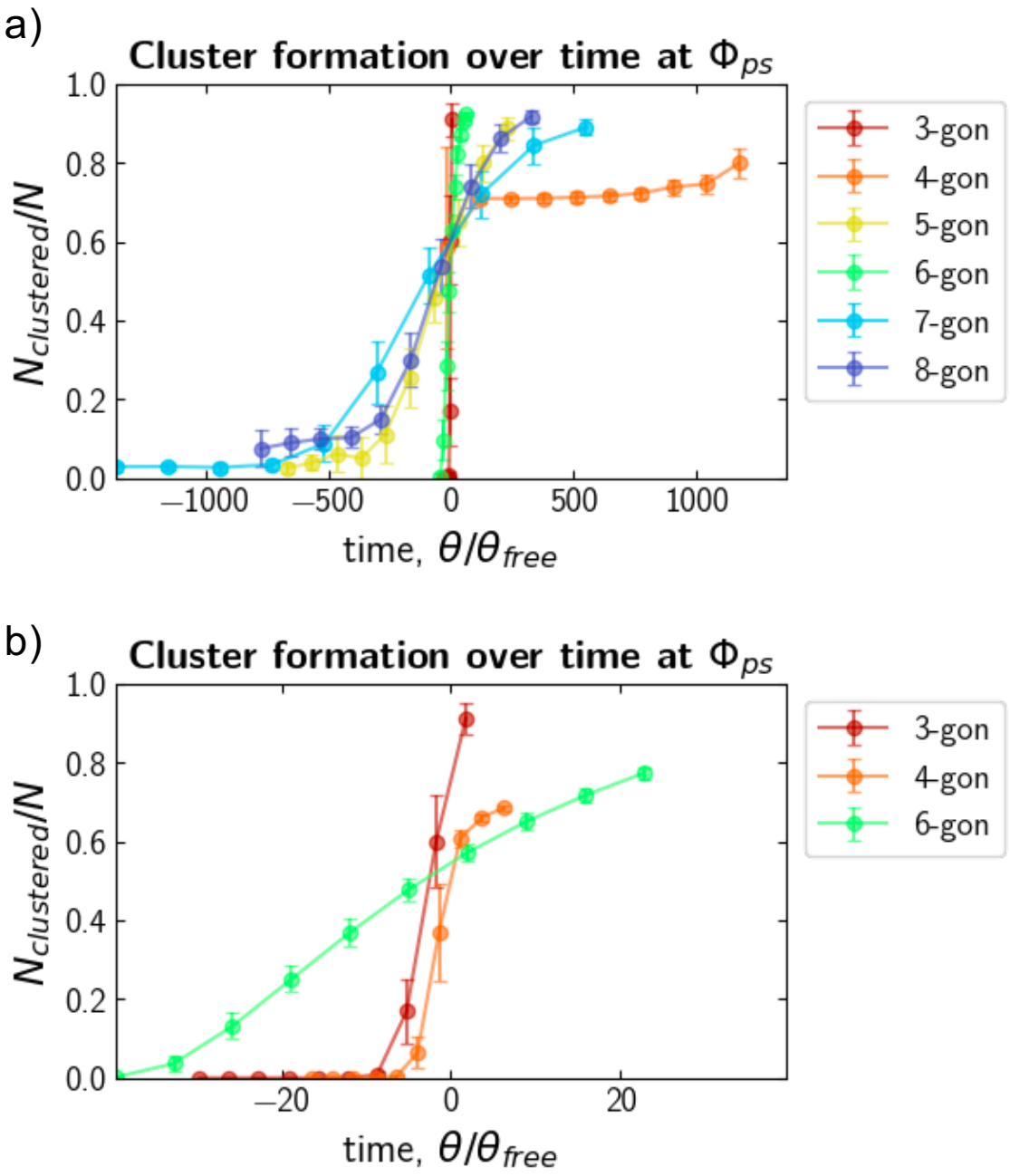

Figure 6.2: Evolution of phase separation in the systems under study. The evolution of the fraction of a system that is in a cluster is plotted versus the normalized time, $\theta/\theta_{\text{free}}$, at the minimum system density of phase separation (Φ_{ps}) a) All studied systems shown for 10k particle systems. We see two major groups of curve collapse: 5-, 7-, and 8-gons, and 3-, 4-, and 6-gons. b) 3-, 4-, and 6-gons in 40k particle systems shown. Even at much shorter timescales than (a), we see that these particle systems display different clustering behavior.

size percolation point [3]. In Figure 6.1, we plot the fraction of replicates at a given Φ that have phase-separated– effectively a $P(\Phi)$– for a set Pe = 150. We see that there is a similarly sharp onset of phase separation to that of a percolation model, even at the system size of 10k particles shown.

Systems with different percolation models can exhibit quantitatively different time evolution of phase separation (e.g. [75, 76]). In Figure 6.2a, we see that at the phase separation density (Φ_{ps}), behavior across all systems collapses onto a few "universal" curves. First, evolving over the largest time ranges, is 5/7/8-gons. In such systems, we see gradual formation of clusters at Φ_{ps}, which can be thought of as the minimum probability to reliably get a percolating cluster in a percolation model. The second group of note is 3- and 4-gons, which near the phase separation transition show rapid phase-separation, highlighted in Figure 6.2b. While these curves follow a similar trajectory and timescale, they do not completely collapse onto one another, warranting further investigation. Finally, relative to the first grouping 6-gons cluster rapidly; but relative to 3- and 4-gons, there is a very gradual increase in the degree of clustering.

We can replicate this behavior at a range of system sizes (2.5k to 40k particles), suggesting that these behaviors are robust outcomes of system preferences and not any system size effects. Further, this difference in phase separation behavior suggests that there are fundamentally different local rules at play in these different types of systems.

6.6 Calculating the cluster scaling distribution

While the previous section investigated the evolution of clustering, we can also investigate the steady-state composition of the systems. In Figure 6.3a, we calculate the cluster size distribution power law exponent, τ_{est} from the distribution at Φ_{ps}. Technically, only at the percolation point p_c will the cluster size distribution be scale free ($n_s \sim s^{-\tau}$). As we do not have a strictly-calculated critical point for the systems

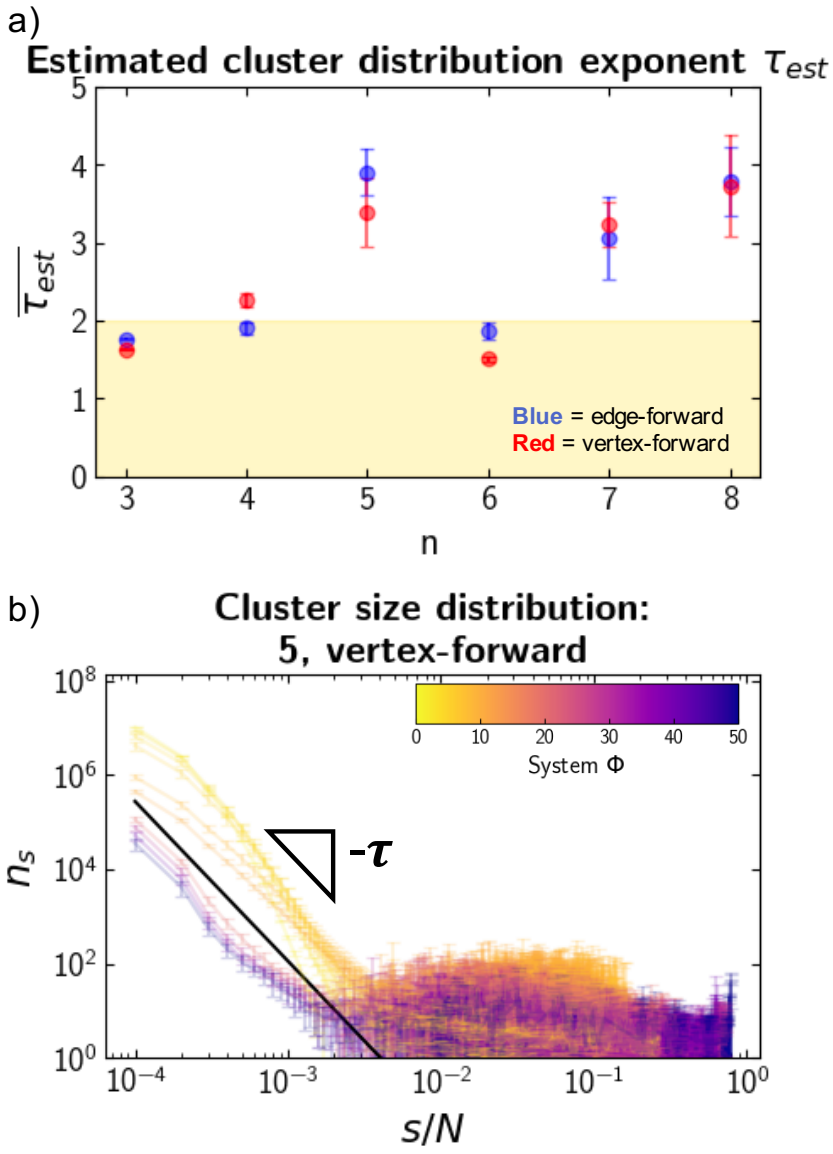

Figure 6.3: Calculation of the estimated power law exponent, τ_{est}, for the cluster size distribution. a) We see that there are two major groupings of behavior in these estimates: 5-, 7-, and 8-gons; and 3-, 4-, and 6-gons. The yellow shaded box highlights τ values below 2, discussed further in the text. b) An example of the quasicritical scaling behavior discussed in the text.

under study, it does not necessarily follow that we would observe scale-free behavior.

Despite not being at the critical point, we see power law behavior in all systems and at a wide variety of system packing fractions, with an example given in Figure 6.3b. Such non-critical power law scaling of cluster size has been reported in other active matter systems [77–79]. In these other studies, this "quasicritical" behavior has been seen in the region of parameter space near the order-disorder transition [80]. It has also led some authors to speculate that the onset of collective motion should be accompanied by a percolation transition. [73]

Additionally, we find our power law behavior falling into the same groupings as seen in Section 6.5: the group of 5-, 7-, and 8-gons with a τ_{est} between 3 and 4, and the group of 3-, 4-, and 6-gons with a τ_{est} of 2 or slightly below. We note that the values of τ found for the second group are possible for systems with "a cutoff in the maximum cluster... size" [81]. Indeed, we've found such behavior at the phase separation density at which 3- and 4-gons form an oscillatory phase in their phase separated regime, and the density at which 6-gons form stable "micro" clusters (Chapter IV). This further suggests that the quantitatively similar behavior found in these groupings may stem from fundamentally different interaction patterns and resulting emergent behavior.

6.7 Conclusions

In previous chapters, we have explored the role of particle shape on the emergent behavior of active particle systems. Here, we proposed mapping active matter near the order-disorder transition onto a non-equilibrium directed percolation model as a means of developing a fundamental framework for understanding the general impact of shape on emergent behavior in non-equilibrium systems. This approach allowed us to identify distinct curve collapses of cluster formation in the 2D polygon systems studied. The groupings of these curve collapses (5-, 7-, and 8-gons; 3- and 4-gons; and 6-gons) mirrors groups with similar densest-packing-facilitated emergent behav-

iors studied in Chapter IV. This suggests that we may be able to generalize this structure-driven emergent behavior as a shared universal behavior within groups. We further explore the critical behavior of these groups and find that the quasicritical behavior of the cluster scaling distribution predicts the same groups as our curve collapses. Further work will be needed to confirm the critical exponents, including a more rigorous finite size scaling approach to identify the critical point of each system.

CHAPTER VII

Conclusions and Future Outlook

The work presented in this thesis answers fundamental questions about the role of shape on the phase separation and emergent behavior in active matter systems. Importantly, these answers raise a number of intriguing questions for the field to consider. I summarize these conclusions and future questions below.

7.1 Conclusions

In Chapter IV, we use systems of 2D active polygons to systematically investigate the impact of particle shape on phase separation. We find that phase separation in such systems is a function of shape, but is not a *monotonic* function of anisotropy. That is, we do not find that as the "roundedness" of a shape increases, that the phase separation density uniformly approaches that of disks. Instead, we find that the phase separation density is closely tied to the densest packing of the component shape, with a lack of shear planes and void space in the densest packings leading to lower system densities of phase separation. We develop a metric of "collision efficiency", whereby we can attribute changes to phase separation density due to shape to the ability of collisions between particles to lead to decreases in particle velocity. We can think of this efficiency as a determinable scaling coefficient on the change in particle velocity with local density ($dv/d\rho$) in MIPS [9].

In Chapter V, we examined one slice of design space at the intersection of system design (stoichiometry) and particle design (particle shape, and to a lesser degree relative size). We demonstrate that this slice of system and particle design space can yield rich system behavior, and highlight three emergent behaviors not yet reported in active matter: microphase separation of species, stable fluid clusters, and a three-phase steady state. We quantify the preferential species attraction leading to the microphase separation as a "steric attraction", representing the ability of effective particle interactions due to shape (even in the absence of explicit attraction terms) to lead to changes in the micro- and macro-scale preferences of a system. We identify the ability of particles to lead to fluidizer behavior as a consequence of disruption to stable cluster formation, showing that increased stoichiometric ratios of the "fluidizer" particles drives shorter cluster lifetimes during the evolution of phase separation. When such clusters collide, the cluster instabilities can balance out and lead to a longer-lived stable fluid cluster. Finally, we show that the fluidizer behavior is a delicate system configuration in that it can also lead to a steady state with coexisting gas, fluid, and solid cluster phases. While the equilibrium concept of a "triple point" does not map onto these non-equilibrium systems, we find it intriguing that we can replicate the triple-phase characteristics of this equilibrium phenomenon in non-equilibrium.

Finally, in Chapter VI we explore the fundamental impact of particle shape on the behavior of active systems by a proposed mapping of active matter near the order-disorder transition onto a non-equilibrium directed percolation model. In doing so, we are able to identify distinct curve collapses of cluster formation in the 2D polygon systems studied, suggesting some degree of shared universal behavior in the groups with shared collapses. We further explore the critical behavior of these groups and find that the quasicritical behavior of the cluster scaling distribution predicts the same groups as our curve collapses. Further work will be needed to confirm the

critical exponents, including a more rigorous finite size scaling approach to identify the critical point of each system.

7.2 Opportunities for future work

7.2.1 Further simulation-based explorations of the active shape design space

In Chapter V, I explored only a slice of the potential design space for active particles. Even in such a narrow slice, we found a rich diversity of emergent behavior. In Chapter II, I presented a framework that could guide further explorations of design space. Systematic explorations, while casting a wide net, may prove useful studies for uncovering fundamental rules governing active matter self-assembly. There are equilibrium analogues for this type of approach, e.g. the exploration of preferred self-assembly of hard shaped particles [82]. Further wide net approaches in active matter could provide data for predictive models or development of theoretical descriptors of the impact of effective inter-particle interactions.

7.2.2 Quantify "temperature" changes due to particle interactions

In a classic equilibrium system, the transition from a fluid to a solid or a gas to a solid at a constant system pressure would be a temperature-driven transition. One thrust of theoretical development in active matter is developing a mapping of thermodynamics from active to equilibrium systems, including the concept of temperature [10, 83]. As active Brownian particles do not exchange kinetic energy, though, such a mapping is not straightforward (for a descriptive example of this, see Section 7 of [83]).

We note that in systems with particle shape, such as those studied in this thesis, a solid dense cluster phase locks out the ability of particles to rotate. In doing

so, the particles are "frozen" out of their ability to rotate freely, in a manner that may be quantifiable as a change in "temperature" (quotations used to indicate that there is not a direct mapping onto our standard equilibrium understanding of such terms). Such changes are also responsible for the formation of a solid, phase-separated cluster. We can imagine other systems in which strong effective particle interactions reduce the ability of particles to reorient freely. While some theories, e.g. "swim temperature"[84], are mapped as a function of density, none yet account for steric or similar effective "freezing" interactions.

Such a theory of steric-induced "temperature" change may also be one way of uniting the collision theory arguments developed in Chapter IV and the steric attraction arguments developed in Chapter V.

7.2.3 Inform experimental design of active particles with tailored behavior through simulation and theory

A challenge in active self-propelled particle systems is that it is not immediately obvious how one would synthesize, to high precision, some of the possible particle designs one could envision. However, that we find such rich behavior even in the simple 2D active polygon models discussed in this thesis should encourage theorists and experimentalists alike that complex particle design is not necessary to achieve complex behavior.

The ultimate realization of the theoretical work in active matter, including this thesis, would be an implementation of an active matter system with tailored emergent behavior to complete a given task. Currently, much of the work in this vein is focused in the colloidal robotics community, where the colloidal "robots" or "molecules" are more complex than the shapes discussed in this thesis [85, 86]. Experimental work validating the emergent behavior of non-isotropic particles (beyond that investigated in [17], as an example) even in seemingly simple active particle systems would provide

a much-needed confirmation of the theoretical work in this area.

While "experimentally realized theory-driven active particle design" remains the widest goal in this "Future work" section, it also represents the final goal I hope this thesis builds towards: experimental realization of active particles with targeted properties.

BIBLIOGRAPHY

BIBLIOGRAPHY

[1] John Towns, Timothy Cockerill, Maytal Dahan, Ian Foster, Andrew Gaither, Kellyand Grimshaw, Victor Hazlewood, Dave Lathrop, Scottand Lifka, Gregory D. Peterson, Ralph Roskies, J. Ray Scott, and Nancy Wilkins-Diehr. Xsede: Accelerating scientific discovery. *Computing in Science Engineering*, 16(5):62–74, Sept.-Oct. 2014.

[2] Alexander Stukowski. Visualization and analysis of atomistic simulation data with OVITO-the Open Visualization Tool. *MODELLING AND SIMULATION IN MATERIALS SCIENCE AND ENGINEERING*, 18(1), JAN 2010.

[3] Dietrich Stauffer and Amnon Aharony. *Introduction to Percolation Theory*. Taylor and Francis, London, UK, 2 edition, 1994.

[4] Sriram Ramaswamy. The mechanics and statistics of active matter. *Annual Review of Condensed Matter Physics*, 1(1):323–345, Aug 2010.

[5] M. C. Marchetti, J. F. Joanny, S. Ramaswamy, T. B. Liverpool, J. Prost, Madan Rao, and R. Aditi Simha. Hydrodynamics of soft active matter. *Reviews of Modern Physics*, 85(3):1143–1189, Jul 2013.

[6] Clemens Bechinger, Roberto Di Leonardo, Hartmut Löwen, Charles Reichhardt, Giorgio Volpe, and Giovanni Volpe. Active particles in complex and crowded environments. *Reviews of Modern Physics*, 88(4), Nov 2016.

[7] M. C. Marchetti, Y. Fily, S. Henkes, A. Patch, and D. Yllanes. Minimal model of active colloids highlights the role of mechanical interactions in controlling the emergent behavior of active matter. *Current Opinion in Colloid & Interface Science*, 21:34–43, 2016.

[8] T. Vicsek, E. Czirók, Ben-Jacob, I. Cohen, and O. Shochet. Novel type of phase transition in a system of self-driven particles. *Physical Review Letters*, 75(6), 1995.

[9] M. E. Cates, D. Marenduzzo, I. Pagonabarraga, and J. Tailleur. Arrested phase separation in reproducing bacteria creates a generic route to pattern formation. *Proceedings of the National Academy of Sciences*, 107(26):11715–11720, 2010.

[10] M. E. Cates and J. Tailleur. When are active brownian particles and run-and-tumble particles equivalent? consequences for motility-induced phase separataion. *Europhysics Letters*, 101(20010), 2013.

[11] Yaouen Fily and M. Cristina Marchetti. Athermal phase separation of self-propelled particles with no alignment. *Physical Review Letters*, 108(23), Jun 2012.

[12] Gabriel S. Redner, Aparna Baskaran, and Michael F. Hagan. Reentrant phase behavior in active colloids with attraction. *Physical Review E*, 88(1), Jul 2013.

[13] Gabriel S. Redner, Michael F. Hagan, and Aparna Baskaran. Structure and dynamics of a phase-separating active colloidal fluid. *Physical Review Letters*, 110(5), Jan 2013.

[14] David Richard, H. Loewen, and Thomas Speck. Nucleation pathway and kinetics of phase-separating active brownian particles. *Soft Matter*, 12:5257–5264, 2016.

[15] Gabriel S. Redner, Caleb G. Wagner, A. Baskaran, and Michael F. Hagan. Classical nucleation theory description of active colloid assembly. *Physical Review Letters*, 117(148002), 2016.

[16] Isaac R. Bruss and Sharon C. Glotzer. Phase separation of self-propelled ballistic particles. *Physical Review E*, 97(042609), 2018.

[17] J. Palacci, S. Sacanna, A. P. Steinberg, D. Pine, and P. M. Chaikin. Living crystals of light-activated colloidal surfers. *Science*, 339:936–940, 2013.

[18] Alexander P. Petroff, Xiao-Lun Wu, and Albert Libchaber. Fast-moving bacteria self-organize into active two-dimensional crystals of rotating cells. *Physical Review Letters*, 114(15), Apr 2015.

[19] G. Briand and O. Dauchot. Crystallization of self-propelled hard discs. *Physical Review Letters*, 117(9), Aug 2016.

[20] H. H. Wensink and H. Loewen. Emergent states in dense systems of active rods: from swarming to turbulence. *Journal of Physics: Condensed Matter*, 24(464130), 2012.

[21] H. H. Wensink, J. Dunkel, S. Heidenreich, K. Drescher, R. E. Goldstein, H. Lowen, and J. M. Yeomans. Meso-scale turbulence in living fluids. *Proceedings of the National Academy of Sciences*, 109(36):14308–14313, Aug 2012.

[22] Yingzi Yang, Vincent Marceau, and Gerhard Gompper. Swarm behavior of self-propelled rods and swimming flagella. *Physical Review E*, 82(3), Sep 2010.

[23] H. H. Wensink, V. Kantsler, R. E. Goldstein, and J. Dunkel. Controlling active self-assembly through broken particle-shape symmetry. *Physical Review E*, 89(1), Jan 2014.

[24] Sven Erik Ilse, Christian Holm, and Joost de Graaf. Surface roughness stabilizes the clustering of self-propelled triangles. *The Journal of Chemical Physics*, 145(13):134904, Oct 2016.

[25] V. Prymidis, S. Samin, and L. Filion. State behaviour and dynamics of self-propelled brownian squares: a simulation study. *Soft Matter*, 2016.

[26] Nguyen H.P. Nguyen, Daphne Klotsa, Michael Engel, and Sharon C. Glotzer. Emergent collective phenomena in a mixture of hard shapes through active rotation. *Physical Review Letters*, 112(7), Feb 2014.

[27] Syeda Sabrina, Matthew Spellings, Sharon C. Glotzer, and Kyle J. M. Bishop. Coarsening dynamics of binary liquids with active rotation. *Soft Matter*, 11(43):8409–8416, 2015.

[28] Matthew Spellings, Michael Engel, Daphne Klotsa, Syeda Sabrina, Aaron M. Drews, Nguyen H. P. Nguyen, Kyle J. M. Bishop, and Sharon C. Glotzer. Shape control and compartmentalization in active colloidal cells. *Proceedings of the National Academy of Sciences*, 112(34):E4642–E4650, Aug 2015.

[29] A. Suma, G. Gonnella, D. Marenduzzo, and E. Orlandini. Motility-induced phase separation in an active dumbbell fluid. *Europhysics Letters*, 108(56004), 2014.

[30] Leticia F. Cugliandolo, Pasquale Digregorio, Giuseppe Gonnella, and Antonio Suma. Phase coexistence in two-dimensional passive and active dumbbell systems. *Physical Review Letters*, 119(26), Dec 2017.

[31] Gerhard Gompper, Roland G Winkler, Thomas Speck, Alexandre Solon, Cesare Nardini, Fernando Peruani, Hartmut Löwen, Ramin Golestanian, U Benjamin Kaupp, Luis Alvarez, Thomas Kiirboe, Eric Lauga, Wilson C K Poon, Antonio DeSimone, Santiago Muiños-Landin, Alexander Fischer, Nicola A Söker, Frank Cichos, Raymond Kapral, Pierre Gaspard, Marisol Ripoll, Francesc Sagues, Amin Doostmohammadi, Julia M Yeomans, Igor S Aranson, Clemens Bechinger, Holger Stark, Charlotte K Hemelrijk, François J Nedelec, Trinish Sarkar, Thibault Aryaksama, Mathilde Lacroix, Guillaume Duclos, Victor Yashunsky, Pascal Silberzan, Marino Arroyo, and Sohan Kale. The 2020 motile active matter roadmap. 32(19):193001, 2020.

[32] Clara del Junco, Laura Tociu, and Suriyanarayanan Vaikuntanathan. Energy dissipation and fluctuations in a driven liquid. *Proceedings of the National Academy of Sciences*, 115(14):3569–3574, 2018.

[33] Thomas Kolb and Daphne Klotsa. Active binary mixtures of fast and slow hard spheres. *Soft Matter*, 2020.

[34] Bryan VanSaders and Sharon C. Glotzer. Pinning dislocations in colloidal crystals with active particles that seek stacking faults. *Soft Matter*, 16(17):4182–4191, 2020.

[35] Sophie Ramananarivo, Etienne Ducrot, and Jeremie Palacci. Activity-controlled annealing of colloidal monolayers. *Nature Communications*, 10(1), July 2019.

[36] B. van der Meer, M. Dijkstra, and L. Filion. Removing grain boundaries from three-dimensional colloidal crystals using active dopants. *Soft Matter*, 12(25):5630–5635, 2016.

[37] S.C. Takatori, W. Yan, and J.F. Brady. Swim pressure: Stress generation in active matter. *Physical Review Letters*, 113(2), Jul 2014.

[38] Isaac R. Bruss and Sharon C. Glotzer. Curvature-induced microswarming. *Soft Matter*, 13:5117–5121, 2017.

[39] Francesco Alaimo, Christian Köhler, and Axel Voigt. Curvature controlled defect dynamics in topological active nematics. *Scientific Reports*, 7(1), July 2017.

[40] Rastko Sknepnek and Silke Henkes. Active swarms on a sphere. *Phys. Rev. E*, 91:022306, Feb 2015.

[41] Sebastian Ehrig, Jonathan Ferracci, Richard Weinkamer, and John W. C. Dunlop. Curvature-controlled defect dynamics in active systems. *Phys. Rev. E*, 95:062609, Jun 2017.

[42] M. Paoluzzi, M. Leoni, and M. C. Marchetti. Fractal aggregation of active particles. *Phys. Rev. E*, 98:052603, Nov 2018.

[43] Mayank Agrawal, Isaac R. Bruss, and Sharon C. Glotzer. Tunable emergent structures and traveling waves in mixtures of passive and contact-triggered-active particles. *Soft Matter*, 13(37):6332–6339, 2017.

[44] Benno Liebchen and Hartmut Löwen. Synthetic chemotaxis and collective behavior in active matter. *Accounts of Chemical Research*, 51(12):2982–2990, 12 2018.

[45] J. Harder, S. A. Mallory, C. Tung, C. Valeriani, and A. Cacciuto. The role of particle shape in active depletion. *The Journal of Chemical Physics*, 141(19):194901, November 2014.

[46] Y. Fily, S. Henkes, and M.C. Marchetti. Freezing and phase separation of self-propelled disks. *Soft Matter*, 10(13):2132–2140, 2014. cited By 129.

[47] John D. Weeks, David Chandler, and Hans C. Andersen. Role of repulsive forces in determining the equilibrium structure of simple liquids. *The Journal of Chemical Physics*, 54(12):5237–5247, Jun 1971.

[48] Carlos Avendaño and Fernando A. Escobedo. Phase behavior of rounded hard-squares. *Soft Matter*, 8(17):4675, 2012.

[49] K. Zhao, R. Bruinsma, and T. G. Mason. Entropic crystal-crystal transitions of brownian squares. *Proceedings of the National Academy of Sciences*, 108(7):2684–2687, Jan 2011.

[50] Kun Zhao and Thomas G. Mason. Frustrated rotator crystals and glasses of brownian pentagons. *Physical Review Letters*, 103(20), Nov 2009.

[51] Matthew Spellings, Ryan L. Marson, Joshua A. Anderson, and Sharon C. Glotzer. Gpu accelerated discrete element method (dem) molecular dynamics for conservative, faceted particle simulations. *Journal of Computational Physics*, 334:460–467, 2017.

[52] Joshua A. Anderson, Chris D. Lorenz, and A. Travesset. General purpose molecular dynamics simulations fully implemented on graphics processing units. *Journal of Computational Physics*, 227(10):5342–5359, May 2008.

[53] Jens Glaser, Trung Dac Nguyen, Joshua A. Anderson, Pak Lui, Filippo Spiga, Jaime A. Millan, David C. Morse, and Sharon C. Glotzer. Strong scaling of general-purpose molecular dynamics simulations on gpus. *Computer Physics Communications*, 192:97–107, 2015.

[54] Carolyn L. Phillips, Joshua A. Anderson, and Sharon C. Glotzer. Pseudo-random number generation for brownian dynamics and dissipative particle dynamics simulations on gpu devices. *Journal of Computational Physics*, 230(19):7191–7201, Aug 2011.

[55] Vyas Ramasubramani, Bradley D. Dice, Eric S. Harper, Matthew P. Spellings, Joshua A. Anderson, and Sharon C. Glotzer. freud: A software suite for high throughput analysis of particle simulation data, 2019.

[56] Carl S. Adorf, Paul M. Dodd, Vyas Ramasubramani, and Sharon C. Glotzer. Simple data and workflow management with the signac framework. *Computational Materials Science*, 146:220 – 229, 2018.

[57] Thomas Kluyver, Benjamin Ragan-Kelley, Fernando Pérez, Brian Granger, Matthias Bussonnier, Jonathan Frederic, Kyle Kelley, Jessica Hamrick, Jason Grout, Sylvain Corlay, Paul Ivanov, Damián Avila, Safia Abdalla, and Carol Willing. Jupyter notebooks – a publishing format for reproducible computational workflows. In F. Loizides and B. Schmidt, editors, *Positioning and Power in Academic Publishing: Players, Agents and Agendas*, pages 87 – 90. IOS Press, 2016.

[58] Pauli Virtanen, Ralf Gommers, Travis E. Oliphant, Matt Haberland, Tyler Reddy, David Cournapeau, Evgeni Burovski, Pearu Peterson, Warren Weckesser, Jonathan Bright, Stéfan J. van der Walt, Matthew Brett, Joshua Wilson, K. Jarrod Millman, Nikolay Mayorov, Andrew R. J. Nelson, Eric Jones, Robert Kern, Eric Larson, CJ Carey, İlhan Polat, Yu Feng, Eric W. Moore, Jake Vand erPlas, Denis Laxalde, Josef Perktold, Robert Cimrman, Ian Henriksen, E. A. Quintero, Charles R Harris, Anne M. Archibald, Antônio H. Ribeiro, Fabian Pedregosa, Paul van Mulbregt, and SciPy 1. 0 Contributors. SciPy 1.0: Fundamental Algorithms for Scientific Computing in Python. *Nature Methods*, 2020.

[59] Travis E Oliphant. *A guide to NumPy*, volume 1. Trelgol Publishing USA, 2006.

[60] Isabella Petrelli, Pasquale Digregorio, Leticia F. Cugliandolo, Giuseppe Gonnella, and Antonio Suma. Active dumbbells: Dynamics and morphology in the coexisting region. *The European Physical Journal E*, 41(10):128, Oct 2018.

[61] Steven Atkinson, Yang Jiao, and Salvatore Torquato. Maximally dense packings of two-dimensional convex and concave noncircular particles. *Physical Review E*, 86(3), Sep 2012.

[62] Robin van Damme, Jeroen Rodenburg, RenÃ© van Roij, and Marjolein Dijkstra. Interparticle torques suppress motility-induced phase separation for rodlike particles. *The Journal of Chemical Physics*, 150(16):164501, 2019.

[63] Previous studies find slightly different critical behavior than we find here. **3-gons:** Very rounded approximations of our edge and vertex forward triangles were able to slide by one another like disks, leading to different phase behavior than we observe (e.g. laning) [23]. In a study of triangles with additional steric interactions due to a rigid-body construction of disks approximating fricitons, vertex-forward simulations also cluster more efficiently than edge-forward triangles, but no quantitative explanation was offered for the oscillatory behavior observed [24]. **4-gons**: The critical density we find for 4-gons is higher than that found in a previous work [25]. This is likely due to two key differences between their methods and ours. First, they set their cut-off for phase separation as the regime where the largest cluster fraction remains higher than 10%, a lower threshhold than we use here. Second, their squares are slightly less round than ours, which we would expect to lead to a lower critical density.

[64] Yan Liu, Yuguang Yang, Bo Li, and Xi-Qiao Feng. Collective oscillation in dense suspension of self-propelled chiral rods. *Soft Matter*, 15:2999–3007, 2019.

[65] Michael P. Howard, Joshua A. Anderson, Arash Nikoubashman, Sharon C. Glotzer, and Athanassios Z. Panagiotopoulos. Efficient neighbor list calculation for molecular simulation of colloidal systems using graphics processing units. *Computer Physics Communications*, 203:45 – 52, 2016.

[66] Fernando Caballero, Cesare Nardini, and Michael E. Cates. From bulk to microphase separtaion in scalar active matter: a perturbative renomalization group analysis. *Journal of Statistical Mechanics: Theory and Experiment*, 123208, 2018.

[67] R.J. Young and P.A. Lovell. *Introduction to Polymers*. CRC Press, second edition, 1991.

[68] Eric S. Harper, Greg van Anders, and Sharon C. Glotzer. The entropic bond in colloidal crystals. *Proceedings of the National Academy of Sciences*, 116(34):16703–16710, 2019.

[69] G. van Anders, D. Klotsa, N.K. Ahmed, Michael Engel, and Sharon C. Glotzer. Understanding shape entropy through local dense packing. *Proceedings of the National Academy of Sciences*, 111(45):E4812–E4821, 2014.

[70] A. P. Solon and J. Tailleur. Flocking with discrete symmetry: The two-dimensional active ising model. *Phys. Rev. E*, 92:042119, Oct 2015.

[71] Benjamin Partridge and Chiu Fan Lee. Critical motility-induced phase separation belongs to the ising universality class. *Physical Review Letters*, 123(068002), August 2019.

[72] Jonathan Tammo Siebert, Florian Dittrich, Friederike Schmid, Kurt Binder, Thomas Speck, and Peter Virnau. Critical behavior of active brownian particles. *Physical Review E*, 98(030601), September 2018.

[73] Nikos Kyriakopoulos, Hugues Chaté, and Francesco Ginella. Clustering and anisotropic correlated percolation in polar flocks. *Physical Review E*, 100(022606), 2019.

[74] Universality classes different from directed percolation. In *Theoretical and Mathematical Physics*, pages 197–259. Springer Netherlands.

[75] Pau Erdős and Alfréd Rényi. On the evolution of random graphs. *Publ. Math. Inst. Hung. Acad. Sci*, 5:17–61, 1960.

[76] Raissa M. D'Souza and Jan Nagler. Anomalous critical and supercritical phenomena in explosive percolation. *Nature Physics*, 11(7):531–538, July 2015.

[77] Hugues Chaté, Francesco Ginelli, Guillaume Grégoire, and Franck Raynaud. Collective motion of self-propelled particles interacting without cohesion. *Phys. Rev. E*, 77:046113, Apr 2008.

[78] F. Peruani, A. Deutsch, and M. Bär. A mean-field theory for self-propelled particles interacting by velocity alignment mechanisms. *The European Physical Journal Special Topics*, 157(1):111–122, April 2008.

[79] Cristián Huepe and Maximino Aldana. Intermittency and clustering in a system of self-driven particles. *Phys. Rev. Lett.*, 92:168701, Apr 2004.

[80] Fernando Peruani and Markus Bär. A kinetic model and scaling properties of non-equilibrium clustering of self-propelled particles. *New Journal of Physics*, 15(6):065009, June 2013.

[81] Hao Hu, Robert M. Ziff, and Youjin Deng. No-enclave percolation corresponds to holes in the cluster backbone. *Phys. Rev. Lett.*, 117:185701, Oct 2016.

[82] Pablo F. Damasceno, Michael Engel, and Sharon C. Glotzer. Predictive self-assembly of polyhedtra into complex structures. *Science*, 337:453–457, 2012.

[83] S. C. Takatori and J.F. Brady. Forces, stresses, and the (thermo?) dynamics of active matter. *Current Opinion in Colloid & Interface Science*, 21:24–33, 2016.

[84] S. C. Takatori and J. F. Brady. Towards a thermodynamics of active matter. *Physical Review E*, 91(3), Mar 2015.

[85] Koohee Han, C. Wyatt Shields, Nidhi M. Diwakar, Bhuvnesh Bharti, Gabriel P. López, and Orlin D. Velev. Sequence-encoded colloidal origami and microbot assemblies from patchy magnetic cubes. *Science Advances*, 3(8), 2017.

[86] Mayank Agrawal and Sharon C. Glotzer. Scale-free, programmable design of morphable chain loops of kilobots and colloidal motors. *Proceedings of the National Academy of Sciences*, 117(16):8700–8710, 2020.